Pentamethylcyclopentadienyl and Cyclopentadienyl Tantalum and Niobium Calixarene Compounds and Their Water and Acetonitrile Inclusion Complexes

Jacqueline A. Acho, Linda H. Doerrer, and Stephen J. Lippard*

Department of Chemistry, Massachusetts Institute of Technology, Cambridge, Massachusetts 02139

Received November 29, 1994[⊗]

The syntheses, spectroscopic properties, crystal and molecular structures, and bonding of several cyclopentadienyl or pentamethylcyclopentadienyl niobium and tantalum calixarene complexes are described. Included are the mononuclear complexes [Cp*Ta(calix[4]arene)] (**1**), [Cp*Ta(*p-tert*-butylcalix[4]arene)] (**2a**), and [CpNb(*p-tert*-butylcalix[4]arene)] (**3**), in which the electron-deficient metal centers are protected in the *exo*-calix position by sterically bulky ligands. These complexes are well suited to bind small-molecule guests within their macrocyclic pockets, as demonstrated in the solid state and in solution for the complexes [Cp*Ta(*p-tert*-butylcalix[4]-arene)]·toluene (**2a**·toluene), [Cp*Ta(OH_2)(*p-tert*-butylcalix[4]arene)] (**2b**), and [Cp*Ta($NCCH_3$)(*p-tert*-butylcalix-[4]arene)] (**2c**). In **1**, the calixarene cavity is elliptically shaped as a result of two sets of *trans*-Ta−O−Ph interbond angles, one wide and one narrow, a geometry that nicely accommodates the toluene guest molecule in **2a**·toluene. In **2b** and **2c**, however, the cavity is cylindrical. Insights into these differences and bonding in these compounds are provided by Fenske−Hall molecular orbital calculations on $[Cp^*Ta]^{4+}[calix[4]arene]^{4-}$, (**1**), a model of **1** with C_{4v} symmetry, [Cp*Ta(OH_2)(calix[4]arene)], and [Cp*Ta($NCCH_3$)(calix[4]arene)]. Crystal data: **1**, monoclinic, $P2_1/c$, a = 11.270(3) Å, b = 18.168(4) Å, c = 15.655(2) Å, β = 110.86(1)°, Z = 4, R = 0.028, R_w = 0.034; **2a**·2toluene·pentane, monoclinic, $P2_1/c$, a = 13.678(2) Å, b = 19.404(2) Å, c = 23.230(2) Å, β = 94.790(9)°, Z = 4, R = 0.030, R_w = 0.038; **2b**, monoclinic, $P2_1/n$, a = 11.168(3) Å, b = 22.211(6) Å, c = 20.957(5) Å, β = 91.17 (1)°, Z = 4, R = 0.031, R_w = 0.037; **2**·2.5CH_2Cl_2, triclinic, $P\bar{1}$ a = 20.21(1) Å, b = 22.70(1) Å, c = 13.346(4) Å, α = 95.10(2)°, β = 97.62(3)°, γ = 108.67(4)°, Z = 4, R = 0.036, R_w = 0.040.

Introduction

Calixarene[1] macrocycles enjoy a long history, but only in the last decade have they captured the attention of transition metal chemists. Investigations of the reactions of phenols with formaldehydes were reported as early as 1872.[2−4] More than a century passed, however, before convenient, high-yield syntheses of the standard calix[*n*]arenes (n = 4, 6, 8) were available.[5] These macrocycles were named "calixarenes" because of the shape of their cone conformation, which is reminiscent of a Grecian *calix*. Two standard representations of tetrameric calixarenes are depicted in Figure 1.

The first transition metal calixarene complexes, [(Ti{*p-tert*-butylcalix[4]arene})$_2$], [(Fe(NH_3){*p-tert*-butylcalix[4]arene-$OSiMe_3$})$_2$], and [(Co_3){*p-tert*-butylcalix[4]arene$OSiMe_3$}$_2$-(THF)], were prepared in the reaction of transition metal (M=Ti, Fe, Co) amides with *p-tert*-butylcalix[4]arene.[6] Other early transition metal calixarene complexes include [{H_2-calix[6]-arene}{$TiCl_2$(μ-O)$TiCl_3$}]$_2$[7] and [M (or RNH_3)][*p-tert*-butylcalix-[8]arene{Ti(O-*i*-Pr)}$_2$].[8,9] These complexes, among other contributions,[10−14] form the basis for transition and lanthanide metal calixarene chemistry.

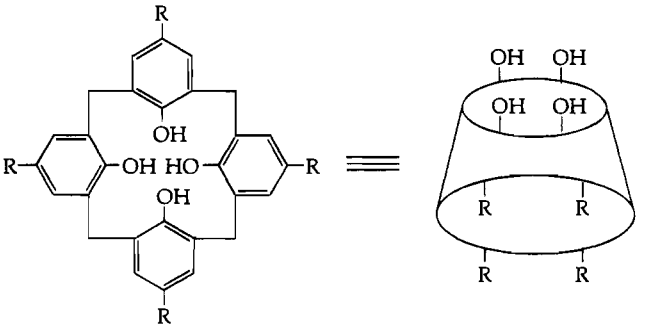

Figure 1. Two representations of calix[4]arenes (calix[4]arene for R = H; *p-tert*-butylcalix[4]arene for R = *tert*-butyl).

Frequently compared to cyclodextrins and cryptands, calixarenes have attracted attention for their ability to include small molecules in the solid state.[15] For example, in the first X-ray structure determination of a calixarene, that of *p-tert*-butylcalix-[4]arene, there was a toluene molecule included in the *endo*-calix position.[16] The ability of the calixarene host to incorporate guest molecules, attributed in part to attractive "alkyl−phenyl"

[⊗] Abstract published in *Advance ACS Abstracts,* April 1, 1995.

(1) Gutsche, C. D. *Calixarenes*; The Royal Society of Chemistry: Cambridge, U.K., 1989; Vol. 1.
(2) Baeyer, A. *Chem. Ber.* **1872**, *5*, 25.
(3) Baeyer, A. *Chem. Ber.* **1872**, *5*, 280.
(4) Baeyer, A. *Chem. Ber.* **1872**, *5*, 1094.
(5) Preparations of standard calix[4,6,8]arenes: (a) Gutsche, C. D.; Iqbal, M. *Org. Synth.*, **1989**, *68*, 234. (b) Gutsche, C. D.; Dhawan, B.; Leonis, M.; Stewart, D. *Org. Synth.* **1989**, *68*, 238. (c) Munch, J. H.; Gutsche, C. D. *Org. Synth.* **1989**, *68*, 243.
(6) Olmstead, M. M.; Sigel, G.; Hope, H.; Xu, X.; Power, P. P. *J. Am. Chem. Soc.* **1985**, *107*, 8087.
(7) Bott, S. G.; Coleman, A. W.; Atwood, J. L. *J. Chem. Soc., Chem. Commun.* **1986**, 610.
(8) Hofmeister, G. E.; Hahn, F. E.; Pedersen, S. F. *J. Am. Chem. Soc.* **1989**, *111*, 2318.
(9) Hofmeister, G. E.; Alvarado, E.; Leary, J. A.; Yoon, D. I.; Pedersen, S. F. *J. Am. Chem. Soc.* **1990**, *112*, 8843.
(10) Furphy, B. M.; Harrowfield, J. M.; Kepert, D. L.; Skelton, B. W.; White, A. H.; Wilner, F. R. *Inorg. Chem.* **1987**, *26*, 4231.
(11) Andreetti, G. D.; Calestani, G.; Ugozzoli, F.; Arduini, A.; Ghidini, E.; Pochini, R.; Ungaro, R. *J. Incl. Phenom.* **1987**, *5*, 123.
(12) Englehardt, L. M.; Furphy, B. M.; Harrowfield, J. M.; Kepert, D. L.; White, A. H.; Wilner, F. R. *Aust. J. Chem.* **1988**, *41*, 1465.
(13) Furphy, B. M.; Harrowfield, J. M.; Ogden, M. I.; Skelton, B. W.; White, A. H.; Wilner, F. R. *J. Chem. Soc., Dalton Trans.* **1989**, 2217.
(14) Corazza, F.; Floriani, C.; Chiesi-Villa, A.; Guastini, C. *J. Chem. Soc., Chem. Commun.* **1990**, 1083.
(15) For some examples, see: (a) Gutsche, C. D. *Acc. Chem. Res.* **1983**, *16*, 161. (b) Gutsche, C. D. *Top. Curr. Chem.* **1984**, *123*, 1. (c) Andreetti, G. D.; Ugozzoli, F.; Ungaro, R.; Pochini, A. In *Inclusion Compounds*; Atwood, J. L., Ed.; Oxford Science: New York, 1984; Vol 4. (d) Atwood, J. L.; Orr, G. W.; Juneja, R. K.; Bott, S. G.; Hamada, F. *Pure Appl. Chem.* **1993**, *65*, 1471.
(16) Andreetti, G. D.; Ungaro, R.; Pochini, A. *J. Chem. Soc., Chem. Commun.* **1979**, 1005.

0020-1669/95/1334-2542$09.00/0

or "$CH_3-\pi$" interactions,[17] extends to transition metal calixarene complexes. The mononuclear compounds [(H_4-*p-tert*-butylcalix[4]arene)(*p-tert*-butylcalix[4]arene)(Mo=O)(H_2O)($PhNO_2$)][18,19] and [(calix[4]arene)(W=O)(CH_3COOH)][14] have open coordination sites directed into the calixarene basket, where solvent is coordinated in the solid state.

The interesting property of the calixarene pocket to include guest molecules, and the relative paucity of transition metal complexes of this ligand, led us to initiate a program to prepare and characterize additional members of the class. Previously we described the synthesis and characterization of novel dimolybdenum(II) calix[4]arene and *p-tert*-butylcalix[4]arene complexes having quadruple bonds. Inclusion of an axially-ligated THF molecule by the calixarene pocket of a neighboring complex helped to organize an extended lattice structure of [$Mo_2(O_2CCH_3)_2$(H_2-*p-tert*-butylcalix[4]arene)(THF)]·C_6H_6 in the solid state.[20] In the present work we examine the inclusion capabilities of discrete niobium and tantalum calixarene complexes. Our aim was to produce mononuclear products with electron-deficient metal centers protected from reaction in the *exo*-calixarene position by sterically-demanding cyclopentadienyl and pentamethylcyclopentadienyl ligands, with available sites for binding nucleophiles at the *endo*-calix site. Here we report the synthesis and characterization of [Cp*Ta(calix[4]-arene)] (**1**), [Cp*Ta(*p-tert*-butylcalix[4]arene)] (**2a**), [CpNb(*p-tert*-butylcalix[4]arene)] (**3**), and the *endo*-calix inclusion complexes [Cp*Ta(OH_2)(*p-tert*-butylcalix[4]arene)] (**2b**) and [Cp*Ta-($NCCH_3$)(*p-tert*-butylcalix[4]arene)] (**2c**).

Experimental Section

General Considerations. All manipulations were carried out in a nitrogen-filled drybox or with standard Schlenk line techniques. Solvents were distilled under nitrogen. Tetrahydrofuran (THF), dimethoxyethane (DME), pentane, toluene, and diethyl ether were distilled from sodium benzophenone ketyl. Methylene chloride and acetonitrile were distilled from CaH_2. Calix[4]arene[21] and *p-tert*-butylcalix[4]arene[5a] were prepared according to published procedures and dried at 130 °C under vacuum for 24 h. Cp*$TaCl_4$ was purchased from Strem Chemicals and purified by washing with benzene and recrystallizing from toluene. CpNbCl_4 was purchased from Strem Chemicals and required no further purification. NMR spectra were obtained on a Varian XL-300 spectrometer at room temperature unless otherwise indicated. All IR spectra were recorded on a Bio-Rad FTS7 Fourier transform instrument. Mass spectra were obtained on a Finnigan 8200 system mass spectrometer.

Preparation of [Cp*Ta(calix[4]arene)] (1). Method A. Calix-[4]arene (200 mg, 0.471 mmol) and Cp*$TaCl_4$ (230 mg, 0.502 mmol) were suspended in 50 mL of toluene in a 100 mL round-bottom flask fitted with a sidearm. The reaction mixture clarified as it was brought to reflux under a flow of argon gas. The evolution of HCl gas, followed by periodically holding moist pH paper over the reaction exhaust, continued for 48 h. The reaction mixture was then allowed to cool to room temperature and was filtered, and the solvent was evaporated. The off-white product **1** (248 mg, 0.337 mmol) was collected in 72% yield.

Method B. Calix[4]arene (100 mg, 0.236 mmol) was deprotonated with 4 equiv of KH (38 mg, 0.947 mmol) in 15 mL of THF. The vigorous effervescence diminished after 1 h, leaving a colorless solution. Cp*$TaCl_4$ (108 mg, 0.236 mmol) was added, producing a yellow color upon dissolution. The reaction mixture was stirred for 3 h and passed through a 1 in. pad of alumina, and the solvent was evaporated. Following a pentane wash and drying in vacuo, the off-white product **1** (99 mg, 0.134 mmol) was collected in 57% yield. Recrystallization by layering pentane onto a toluene solution of **1** at −40 °C afforded X-ray-quality crystals. IR (KBr): 3001 (w), 2962 (w), 2947 (w), 2919 (m), 1588 (m), 1464 (vs), 1448 (vs), 1426 (s), 1310 (sh), 1293 (s), 1270 (vs), 1256 (s), 1244 (sh), 1221 (s), 1203 (s), 1083 (m), 1070 (m), 935 (m), 921 (s), 882 (m), 860 (m), 847 (m), 835 (m), 751 (vs), 744 (sh), 727 (m), 698 (m), 597 (w), 577 (w), 532 (m), 514 (m) cm^{-1}. ^1H NMR ($CDCl_3$, 300 MHz): δ 2.49 (s, 15H; Cp*(Me)), 3.20 (d, J = 12 Hz, 4H; CH_2), 4.32 (d, J = 12 Hz, 4H; CH_2), 6.60 (t, J = 6 Hz, 4H; Ph), 6.97 (d, J = 6 Hz, 8H; Ph) ppm. MS(EI): 736 (M^+, 100), 601 ([M − Cp*]$^+$, 58), 368 (28), 351 (8). Anal. Calcd for $C_{38}H_{35}O_4Ta$ (**1**): C, 61.96; H, 4.79. Found: C, 61.55; H, 4.85.

Preparation of [Cp*Ta(*p-tert*-butylcalix[4]arene)] (2a). Method A. A vigorously stirred suspension of Cp*$TaCl_4$ (318 mg, 0.694 mmol) and *p-tert*-butylcalix[4]arene (550 mg, 0.742 mmol) was brought to reflux in 50 mL of toluene under a purge of argon gas. The resulting solution evolved HCl gas, which could be monitored by holding moist pH paper over the exhaust of reaction; acid production ceased after 48 h. Evaporation of the solvent left a light yellow powder, **2a** (621 mg, 0.646 mmol), in 93% yield. The crude product was judged to be >95% pure by its ^1H NMR spectrum and could be recrystallized by vapor diffusion of pentane into a toluene solution of **2a** to give crystals suitable for X-ray diffraction studies.

Method B. *p-tert*-Butylcalix[4]arene (250 mg, 0.337 mmol) was deprotonated by an excess of KH (78 mg, 1.94 mmol) in 15 mL of DME. The suspension clarified then developed a fluffy white precipitate. Gas evolution ceased after 1 h of vigorous stirring. To the resulting white suspension was added Cp*$TaCl_4$ (200 mg, 0.437 mmol). The reaction mixture clarified and turned deep orange as it was stirred over 12 h. After concentration of the orange solution to dryness, extraction of the resulting solid with CH_2Cl_2, and evaporation of the solvent from the filtrate, the light yellow product **2a** (244 mg, 0.254 mmol) was obtained in 58% yield. IR (KBr): 3038 (sh), 2952 (vs, br), 1471 (vs), 1365 (m), 1311 (s), 1254 (s), 1204 (vs), 1110 (m), 1027 (w), 924 (m), 873 (m), 834 (m), 794 (m), 763 (w), 736 (w), 543 (m), 429 (sh), 403 (m) cm^{-1}. ^1H NMR ($CDCl_3$, 300 MHz): δ 1.19 (s, 36H; *t*-Bu), 2.46 (s, 15H; Cp*(Me)), 3.18 (d, J = 12 Hz, 4H; CH_2), 4.34 (d, J = 12 Hz, 4H; CH_2), 7.01 (s, 8H; Ph) ppm. MS(EI): 961 (M^+, 100), 946 ([M − CH_3]$^+$, 62), 904 ([M − (*t*-Bu)]$^+$, 2), 465 (40). Anal. Calcd for $C_{54}H_{67}O_4Ta$ (**2a**): C, 67.49; H, 7.03. Found: C, 67.18; H, 7.10.

Preparation of [Cp*Ta(OH_2)(*p-tert*-butylcalix[4]arene)] (2b). Dissolution of complex **2a** in wet acetone, followed by slow evaporation of solvent and filtration, produced X-ray-quality crystals of complex **2b** in essentially quantitative yield. IR (KBr): 3480 (m), 3425 (m), 3036 (m), 2954 (s), 2914 (sh), 1715 (m), 1595 (w), 1459 (vs), 1427 (sh), 1361 (m), 1305 (s), 1255 (sh), 1203 (s), 1116 (m), 1023 (w), 919 (m), 873 (m), 830 (s), 796 (m), 761 (m), 678 (w), 543 (m), 498 (w), 417 (m) cm^{-1}. ^1H NMR ($CDCl_3$, 300 MHz): δ 1.19 (s, 36H; *t*-Bu), 2.16 (s, 6H; $(CH_3)_2CO$), 2.23 (br, 2H; Ta−OH_2), 2.41 (s, 15H; Cp*-(Me)), 3.14 (d, J = 12 Hz, 4H; CH_2), 4.25 (d, J = 12 Hz, 4H; CH_2), 7.01 (s, 8H; Ph) ppm. Anal. Calcd for $C_{57}H_{75}O_6Ta$ (**2b**·acetone): C, 66.01; H, 7.29. Found: C, 65.59; H, 7.26.

Preparation of [Cp*Ta($NCCH_3$)(*p-tert*-butylcalix[4]arene)] (2c). Complex **2a** (200 mg, 0.208 mmol) was dissolved in 10 mL of CH_2Cl_2. When 3 mL of CH_3CN was added dropwise to the light yellow reaction solution, the color bleached and a waxy white precipitate developed. Additional CH_2Cl_2 was added to dissolve the precipitate. Cooling the colorless solution for several hours at −30 °C produced the first crop of large X-ray-quality block-shaped crystals which were filtered off, crushed, and dried in vacuo. Concentration and cooling of the mother liquor afforded more crystals, resulting in a 94% (196 mg, 0.196 mmol) overall yield. IR (KBr): 2954 (vs, br), 2920 (vs, br), 2864 (vs, br), 2714 (w), 2332 (s), 2302 (m), 1480 (vs), 1392 (s), 1360 (vs), 1307 (vs), 1258 (vs), 1206 (vs), 1162 (sh), 1128 (s), 1107 (s), 1024 (m), 950 (m), 919 (vs), 888 (m), 871 (s), 833 (vs), 800 (vs), 763 (s), 678 (m), 588 (m), 543 (vs), 500 (s) cm^{-1}. ^1H NMR ($CDCl_3$, 300 MHz): δ −0.28 (br, 3H; Ta−$NCCH_3$), 1.19 (s, 36H; *t*-Bu), 2.44 (s, 15H; Cp*(Me)), 3.16 (d, J = 12 Hz, 4H; CH_2), 4.26 (d, J = 12 Hz, 4H; CH_2), 5.29 (s, CH_2Cl_2), 7.09 (s, 8H; Ph) ppm. Anal. Calcd for

(17) Andreetti, G. D.; Ori, O.; Ugozzoli, F.; Alfieri, C.; Pochini, A.; Ungaro, R. *J. Incl. Phenom.* **1988**, *6*, 523.
(18) Corazza, F.; Floriani, C.; Chiesi-Villa, A.; Guastini, C. *J. Chem. Soc., Chem. Commun.* **1990**, 640.
(19) Corazza, F.; Floriani, C.; Chiesi-Villa, A.; Rizzoli, C. *Inorg. Chem.* **1991**, *30*, 4465.
(20) Acho, J. A.; Lippard, S. J. *Inorg. Chim. Acta.* **1995**, *229*, 5.
(21) Gutsche, C. D.; Levine, J. A.; Sujeeth, P. K. *J. Org. Chem.* **1985**, *50*, 5802.

Table 1. X-ray Crystallographic Information for [Cp*Ta(calix[4]arene)] (**1**), [Cp*Ta(*p-tert*-butylcalix[4]-arene)]·2toluene·pentane (**2a**·2toluene·pentane), [Cp*Ta(OH$_2$)(*p-tert*-butylcalix[4]arene)]·acetone (**2b**·acetone), and [Cp*Ta(NCCH$_3$)(*p-tert*-butylcalix[4]arene)]·2.5CH$_2$Cl$_2$ (**2c**·2.5CH$_2$Cl$_2$)[a]

	1	**2a**·2toluene·pentane	**2b**·acetone	**2c**·2.5CH$_2$Cl$_2$
formula	$C_{38}H_{35}O_4Ta$	$C_{71}H_{83}O_4Ta$	$C_{57}H_{75}O_6Ta$	$C_{58.5}H_{75}NO_4Cl_5Ta$
a (Å)	11.270(3)	13.678 (2)	11.168(3)	20.21(1)
b (Å)	18.168(4)	19.404 (2)	22.211(6)	22.70(1)
c (Å)	15.655(2)	23.230 (2)	20.957(5)	13.346(4)
α (deg)				95.10(2)
β (deg)	110.86(1)	94.790 (9)	91.17(1)	97.62(3)
γ (deg)				108.67(4)
V (Å^3)	2995(1)	6144 (1)	4963(2)	5691(4)
T (°C)	−83.1	−73.8	−78.1	−110
fw	736.64	1181.38	961.16	1214.46
Z	4	4	4	4
ϱ_{calc} (g/cm^3)	1.63	1.28	1.39	1.42
space group	$P2_1/c$	$P2_1/c$	$P2_1/n$	$P\bar{1}$
2θ limits (deg)	3−50	3−51	3−50	3−50
data limits	$+h,+k,\pm l$	$+h,+k,\pm l$	$+h,+k,\pm l$	$+h,\pm k,\pm l$
μ (cm^{-1})	37.07	18.32	22.35	22.08
no. of total data	5862	12585	11039	21134
no. of unique data	5480	11995	8970	19825
R(merge)[b]	3.0	5.1	2.8	2.5
no. of unique obsd[c] data	4184	8636	6798	14108
no. of LS params	388	670	577	1252
p factor	0.03	0.03	0.03	0.03
R[d]	0.028	0.030	0.031	0.036
R_w	0.034	0.038	0.037	0.040

[a] Data were collected on an Enraf-Nonius CAD-4F κ geometry diffractometer using Mo Kα radiation. [b] R(merge) = $\sum_{i=1}^{n}\sum_{j=1}^{m}|\langle F_i^2\rangle - F_{ij}^2|/\sum_{i=1}^{n}m\langle F_i^2\rangle$ where n = number of reflections observed more than once, m = number of times a given reflection was observed, and $\langle F_i^2\rangle$ is the average value of F^2 for reflection i. [c] Observation criterion $I > 3\sigma(I)$. [d] $R = \sum||F_o| - |F_c||/\sum|F_o|$, $R_w = [\sum w(|F_o| - |F_c|)^2/\sum w|F_o|^2]^{1/2}$, where $w = 1/\sigma^2(F)$, as defined in: Carnahan, E. M.; Rardin, R. L.; Bott, S. G.; Lippard, S. J. *Inorg. Chem.* **1992**, *31*, 5193.

$C_{56.5}H_{71}O_4NClTa$ (**2c**·0.5CH$_2$Cl$_2$): C, 64.97; H, 6.85; N, 1.34. Found: C, 64.52; H, 6.65; N, 1.64.

Preparation of [CpNb(*p-tert*-butylcalix[4]arene)] (3). Method A. *p-tert*-Butylcalix[4]arene (500 mg, 0.736 mmol) and CpNbCl$_4$ (221 mg, 0.737 mmol) were loaded into a 200 mL round-bottom flask fitted with a sidearm and suspended in 100 mL of toluene. The rust-colored reaction solution clarified and evolved HCl as it was brought to reflux under a flow of argon gas. The reaction mixture was refluxed for 2 days, during which time the color faded to yellow. The solvent was removed in vacuo, and the crude product was extracted into diethyl ether. Filtration, followed by evaporation of the ether, afforded the yellow product **3** (426 mg, 0.530 mmol) in 72% yield.

Method B. *p-tert*-Butylcalix[4]arene (100 mg, 0.135 mmol) was deprotonated with 4 equiv of KH (22 mg, 0.548 mmol) in THF over 1 h. CpNbCl$_4$ (40 mg, 0.133 mmol) was added to the reaction flask, and the reaction mixture was stirred for 2 h. The resulting yellow-brown solution was passed through a 1 in. pad of alumina and the solvent was evaporated. The yellow product **3** (73 mg, 0.091 mmol) was isolated in 68% yield. The product could be recrystallized from pentane at −40 °C. IR (KBr): 3420 (m), 2956 (s), 2913 (sh), 2870 (sh), 1752 (w), 1561 (m), 1463 (vs), 1402 (sh), 1364 (w), 1294 (s), 1255 (sh), 1202 (s), 1114 (m), 1077 (sh), 1026 (w), 920 (m), 876 (m), 821 (vs), 763 (m), 676 (w), 575 (sh), 548 (s), 498 (m), 421 (s) cm^{-1}. ^{1}H NMR (CDCl$_3$, 300 MHz): δ 1.19 (s, 36H; *t*-Bu), 3.15 (d, J = 12 Hz, 4H; CH$_2$), 4.37 (d, J = 12 Hz, 4H; CH$_2$), 7.00 (s, 8H; Ph), 7.06 (s, 5H; Cp) ppm. MS(EI): 802 (M$^+$, 100), 787 ([M − CH$_3$]$^+$, 67), 386 (34). Anal. Calcd for $C_{49}H_{57}O_4Nb$ (3): C, 73.30; H, 7.16. Found: C, 73.27; H, 7.14.

Table 2. Final Positional Parameters and B(eq) Values for [Cp*Ta(calix[4]arene)], **1**[a]

atom	x	y	z	B(eq)[b] (Å^2)
Ta	0.272613(19)	0.170703(10)	0.255635(13)	1.336(8)
O(20)	0.43571(34)	0.19934(19)	0.33792(24)	2.3(1)
O(40)	0.24878(31)	0.27897(18)	0.22866(21)	1.6(1)
O(60)	0.11815(38)	0.17836(20)	0.27442(29)	2.9(2)
O(80)	0.29900(34)	0.08092(18)	0.33415(22)	1.9(1)
C(1)	0.33845(58)	0.16962(29)	0.12416(35)	2.4(2)
C(2)	0.20398(58)	0.17678(29)	0.08891(34)	2.4(2)
C(3)	0.14909(52)	0.11117(30)	0.10848(34)	2.1(2)
C(4)	0.25122(50)	0.06265(26)	0.15441(33)	1.7(2)
C(5)	0.36752(51)	0.09917(29)	0.16583(34)	2.0(2)
C(6)	0.43237(75)	0.22438(35)	0.11549(47)	4.0(3)
C(7)	0.13385(80)	0.24118(36)	0.03456(42)	4.6(3)
C(8)	0.01202(59)	0.09430(37)	0.08075(43)	3.7(3)
C(9)	0.23853(54)	−0.01407(30)	0.18329(38)	2.5(2)
C(10)	0.49769(59)	0.06804(33)	0.20926(44)	3.2(3)
C(20)	0.52714(47)	0.22576(28)	0.41247(33)	1.6(2)
C(21)	0.58726(48)	0.17743(28)	0.48493(35)	1.9(2)
C(22)	0.68451(54)	0.20552(32)	0.56024(36)	2.6(2)
C(23)	0.71916(56)	0.27902(35)	0.56468(39)	3.0(2)
C(24)	0.65661(54)	0.32531(31)	0.49231(40)	2.6(2)
C(25)	0.55986(47)	0.29984(29)	0.41543(35)	1.8(2)
C(26)	0.48276(50)	0.34960(28)	0.33936(35)	1.9(2)
C(40)	0.24296(48)	0.33069(27)	0.29034(33)	1.6(2)
C(41)	0.35483(48)	0.36752(26)	0.34471(32)	1.6(2)
C(42)	0.34699(53)	0.42050(29)	0.40710(36)	2.3(2)
C(43)	0.23326(56)	0.43784(30)	0.41560(38)	2.6(2)
C(44)	0.12445(52)	0.40283(30)	0.36044(37)	2.4(2)
C(45)	0.12519(50)	0.34971(28)	0.29764(34)	1.9(2)
C(46)	0.00120(52)	0.31506(30)	0.23768(36)	2.2(2)
C(60)	0.01649(47)	0.18765(30)	0.30029(35)	1.9(2)
C(61)	−0.04549(47)	0.25464(31)	0.28432(34)	2.0(2)
C(62)	−0.14692(57)	0.26267(35)	0.31390(42)	3.1(3)
C(63)	−0.18408(60)	0.20496(41)	0.35740(49)	3.8(3)
C(64)	−0.12036(58)	0.13874(37)	0.37206(44)	3.3(3)
C(65)	−0.01652(51)	0.12834(31)	0.34603(37)	2.3(2)
C(66)	0.06232(56)	0.05893(31)	0.36382(40)	2.6(2)
C(80)	0.30328(53)	0.07995(26)	0.42323(34)	1.9(2)
C(81)	0.18972(54)	0.06714(27)	0.43931(36)	2.1(2)
C(82)	0.19904(60)	0.06187(30)	0.53068(40)	2.7(2)
C(83)	0.31331(66)	0.06949(31)	0.60207(40)	3.1(3)
C(84)	0.42257(59)	0.08184(30)	0.58440(37)	2.7(2)
C(85)	0.41931(53)	0.08779(27)	0.49500(36)	2.1(2)
C(86)	0.54392(54)	0.09807(29)	0.47887(36)	2.4(2)

[a] Numbers in parentheses are estimated standard deviations of the last significant figure. See Figure 3 for atom-labeling scheme. [b] B(eq) = $^4/_3[a^2\beta_{11} + b^2\beta_{22} + c^2\beta_{33} + 2ab(\cos\gamma)\beta_{12} + 2ac(\cos\beta)\beta_{13} + 2bc(\cos\alpha)\beta_{23}]$.

X-ray Crystallography. General Procedures. Details of the crystal data and the data collection parameters for **1** and **2a**−**c** are reported in Table 1. Intensity data were collected on an Enraf-Nonius CAD-4 diffractometer by using graphite-monochromated Mo Kα radiation and methods previously described.[22] Unit cell parameters were determined and refined from 25 reflections with $2\theta > 20°$. All data were corrected for Lorentz and polarization effects. The observed structure factors for equivalent reflections were averaged.

[Cp*Ta(calix[4]arene)] (1). Very pale yellow crystals grew when pentane was allowed to diffuse slowly into a toluene solution of **1**. A rod of dimensions 0.2 × 0.2 × 0.5 was mounted vertically on the end of a quartz fiber with silicone grease. The crystal was transferred to the diffractometer and studied at low temperature. Crystal quality was determined to be good from axial photographs and open-counter ω-scans of several low-angle reflections ($\Delta\bar{\omega}_{1/2} = 0.24°$) which showed no fine structure. The crystal had 2/*m* Laue symmetry and systematic absences consistent with the centrosymmetric space group $P2_1/c$. Each asymmetric unit contains one molecule of **1**. There are no solvent molecules in the lattice. The tantalum and oxygen atoms were located by direct methods. All other non-hydrogen atoms were found through least-squares refinement and difference Fourier procedures. Hydrogen atoms were generated and fixed to ride on attached carbon atoms (d_{C-H}

(22) Carnahan, E. M.; Rardin, R. L.; Bott, S. G.; Lippard, S. J. *Inorg. Chem.* **1992**, *31*, 5193.

= 0.95 Å, $B_H = 1.2B_C$). The largest residual peak found in the final difference Fourier map was 1.1 e/Å^3, located at a distance of 1.03 Å from the tantalum atom. Final positional parameters for non-hydrogen atoms are given in Table 2.

[Cp*Ta(*p-tert*-butylcalix[4]arene)] (2a). Very pale yellow crystals were grown from slow diffusion of pentane into a toluene solution of **2a** at −40 °C. A block-shaped specimen of dimensions 0.5 × 0.4 × 0.3 mm was transferred to a liquid nitrogen cold stage and mounted with silicone grease on the tip of a quartz fiber. The crystal was transferred to the diffractometer and studied at low temperature, revealing 2/*m* Laue symmetry. Crystal quality was judged to be acceptable on the basis of axial photographs and open-counter ω-scans of several low-angle reflections with $\Delta\bar{\omega}_{1/2} = 0.23°$ and no fine structure. Systematic absences were consistent with the space group $P2_1/c$. An empirical ψ-scan absorption correction was applied to the data. The positions of the tantalum and oxygen atoms were determined by direct methods. All other non-hydrogen atoms were located by a series of least-squares refinements and difference Fourier techniques. In the asymmetric unit, there are one molecule of **2a**, two molecules of toluene, and one molecule of pentane. All non-hydrogen atoms except for those of the pentane molecule were allowed to refine anisotropically. The carbon atoms of the lattice pentane molecule were refined isotropically. The central carbon in the pentane is disordered over two positions related by a crystallographic inversion center. A two-site model was introduced for these positions with 50% occupancy each. All hydrogen atoms were placed in calculated positions and fixed to the attached carbon atoms ($d_{C-H} = 0.95$ Å, $B_H = 1.2\,B_C$). The largest residual peak in the final difference Fourier map was 0.7 e/Å^3, located at a distance of 0.72 Å from the C(208) of the pentane molecule in the lattice. Non-hydrogen atomic positional parameters are given in Table 3.

[Cp*Ta(OH$_2$)(*p-tert*-butylcalix[4]arene)] (2b). Colorless crystals of **2b** were grown by slow evaporation of a moist acetone solution of **2a**. A parallelepiped of **2b** (dimensions 0.25 × 0.40 × 0.40 mm) was mounted on the end of a quartz fiber in Paratone N oil (EXXON). The crystal was judged to be acceptable on the basis of open-counter ω-scans of several low-angle reflections ($\Delta\bar{\omega}_{1/2} = 0.21°$; no fine structure) and by axial photographs. Examination on the diffractometer revealed 2/*m* Laue symmetry and systematic absences consistent with space group $P2_1/n$.[23] A ψ-scan absorption correction was applied to the data. The tantalum atom was found by direct methods. All remaining non-hydrogen atoms were located by subsequent least-squares refinements and difference Fourier maps. Hydrogen atoms H(1) and H(2) were located on the difference map and refined isotropically. The remaining hydrogen atoms were placed in calculated positions and fixed to the attached carbon atoms ($d_{C-H} = 0.95$ Å, $B_H = 1.2\,B_C$). The largest residual peak in the final difference Fourier map was 1.6 e/Å^3, located at a distance of 0.97 Å from the tantalum atom. Final atomic positional parameters for all refined atoms are given in Table 4.

[Cp*Ta(NCCH$_3$)(*p-tert*-butylcalix[4]arene)] (2c). Large blocks of colorless crystals of **2c** grew overnight at −40 °C from a CH_2Cl_2/$NCCH_3$ solution of **2a**. An irregular crystal of dimensions 0.5 × 0.3 × 0.3 mm was covered in Paratone N and maneuvered onto the end of a quartz fiber. Study on the diffractometer at low temperature indicated a triclinic crystal system. Quality of the crystal was judged to be good on the basis of axial photographs and open-counter ω-scans of several low-angle reflections ($\Delta\bar{\omega}_{1/2} = 0.24°$; no fine structure). Intensity statistics indicated the centrosymmetric space group $P\bar{1}$. An empirical ψ-scan absorption correction was applied to the data. Tantalum and oxygen atom positions were determined by direct methods. All other non-hydrogen atoms were located by iterative least-squares refinements and difference Fourier procedures. Hydrogen atom positions were calculated and fixed to ride on attached carbon atoms ($d_{C-H} = 0.95$ Å, $B_H = 1.2\,B_C$). Final refinement yielded the residuals given in Table 1. The largest residual peak found in the final difference Fourier map was 1.0 e/Å^3, located at a distance of 1.01 Å from the tantalum atom. Final positional parameters are given in Table 5.

Fenske−Hall Calculations. Nonempirical Fenske−Hall molecular orbital calculations[24] were carried out on a VAX 4000-90 workstation.

(23) *International Tables for Crystallography*; Hahn, T., Ed.; Kluwer Academic Publishers: Dordrecht, The Netherlands, 1989; Vol. A.

Table 3. Final Positional Parameters and *B*(eq) Values for [Cp*Ta(*p-tert*-butylcalix[4]arene)]·2toluene·pentane, **2a**·2toluene·pentane[a]

atom	*x*	*y*	*z*	*B*(eq)[b] (Å^2)
Ta	1.26382(1)	−0.091543(8)	0.582985(7)	1.323(7)
O(20)	1.3421(2)	−0.1606(1)	0.6198(1)	1.9(1)
O(40)	1.2940(2)	−0.0421(1)	0.6582(1)	1.6(1)
O(60)	1.1311(2)	−0.0765(2)	0.5965(1)	2.2(1)
O(80)	1.2124(2)	−0.1692(1)	0.5325(1)	1.7(1)
C(1)	1.4031(3)	−0.0553(2)	0.5306(2)	1.9(2)
C(2)	1.3726(3)	0.0033(2)	0.5604(2)	2.1(2)
C(3)	1.2768(3)	0.0207(2)	0.5381(2)	2.2(2)
C(4)	1.2477(3)	−0.0264(2)	0.4929(2)	2.1(2)
C(5)	1.3270(3)	−0.0722(2)	0.4876(2)	1.8(2)
C(6)	1.5001(3)	−0.0903(3)	0.5413(2)	2.9(2)
C(7)	1.4333(4)	0.0430(3)	0.6057(2)	3.5(2)
C(8)	1.2174(5)	0.0809(3)	0.5569(2)	3.7(3)
C(9)	1.1507(4)	−0.0285(3)	0.4573(2)	3.0(2)
C(10)	1.3294(4)	−0.1272(3)	0.4428(2)	2.5(2)
C(20)	1.4000(3)	−0.2102(2)	0.6451(2)	1.7(2)
C(21)	1.4044(3)	−0.2735(2)	0.6167(2)	1.9(2)
C(22)	1.4668(3)	−0.3232(2)	0.6425(2)	2.1(2)
C(23)	1.5226(3)	−0.3117(2)	0.6944(2)	2.3(2)
C(24)	1.5125(3)	−0.2482(2)	0.7215(2)	2.0(2)
C(25)	1.4520(3)	−0.1962(2)	0.6974(2)	1.5(2)
C(26)	1.4432(3)	−0.1248(2)	0.7232(2)	1.7(2)
C(27)	1.5913(4)	−0.3692(3)	0.7197(2)	2.9(2)
C(28)	1.6609(5)	−0.3916(4)	0.6747(3)	5.5(3)
C(29)	1.6538(4)	−0.3469(3)	0.7738(2)	3.7(3)
C(30)	1.5290(5)	−0.4310(3)	0.7352(3)	4.4(3)
C(40)	1.2738(3)	−0.0676(2)	0.7107(2)	1.5(2)
C(41)	1.3434(3)	−0.1075(2)	0.7437(2)	1.7(2)
C(42)	1.3218(3)	−0.1297(2)	0.7981(2)	1.8(2)
C(43)	1.2341(3)	−0.1147(2)	0.8214(2)	1.8(2)
C(44)	1.1671(3)	−0.0754(2)	0.7874(2)	1.9(2)
C(45)	1.1850(3)	−0.0517(2)	0.7327(2)	1.5(2)
C(46)	1.1067(3)	−0.0077(2)	0.6996(2)	1.9(2)
C(47)	1.2147(3)	−0.1357(2)	0.8833(2)	2.3(2)
C(48)	1.2449(5)	−0.0765(3)	0.9240(2)	4.6(3)
C(49)	1.1072(4)	−0.1517(3)	0.8886(3)	4.5(3)
C(50)	1.2719(5)	−0.1997(3)	0.9026(2)	4.6(3)
C(60)	1.0441(3)	−0.0861(2)	0.6196(2)	1.9(2)
C(61)	1.0261(3)	−0.0504(2)	0.6688(2)	1.8(2)
C(62)	0.9344(3)	−0.0584(3)	0.6898(2)	2.3(2)
C(63)	0.8629(3)	−0.1012(2)	0.6637(2)	2.5(2)
C(64)	0.8863(3)	−0.1380(2)	0.6153(2)	2.4(2)
C(65)	0.9765(3)	−0.1317(2)	0.5920(2)	2.0(2)
C(66)	1.0032(3)	−0.1733(2)	0.5413(2)	2.3(2)
C(67)	0.7607(4)	−0.1059(3)	0.6866(2)	3.3(2)
C(68)	0.7118(4)	−0.0354(4)	0.6813(4)	6.0(4)
C(69)	0.6949(4)	−0.1571(4)	0.6518(3)	5.7(4)
C(70)	0.7701(5)	−0.1298(4)	0.7483(3)	5.6(4)
C(80)	1.1735(3)	−0.2277(2)	0.5533(2)	1.7(2)
C(81)	1.0723(3)	−0.2321(2)	0.5581(2)	1.9(2)
C(82)	1.0344(3)	−0.2929(2)	0.5789(2)	2.5(2)
C(83)	1.0918(4)	−0.3501(2)	0.5942(2)	2.5(2)
C(84)	1.1911(4)	−0.3446(2)	0.5875(2)	2.3(2)
C(85)	1.2335(3)	−0.2850(2)	0.5674(2)	1.8(2)
C(86)	1.3424(3)	−0.2837(2)	0.5606(2)	1.9(2)
C(87)	1.0462(4)	−0.4180(3)	0.6128(2)	3.4(2)
C(88)	1.031(1)	−0.4625(4)	0.5626(3)	14.3(8)
C(89)	1.1113(6)	−0.4537(4)	0.6603(4)	8.0(5)
C(90)	0.9484(7)	−0.4069(4)	0.6381(5)	10.3(6)
C(100)	1.2740(6)	−0.3240(5)	0.7595(4)	7.8(5)
C(101)	1.1721(5)	−0.3111(4)	0.7681(3)	5.2(4)
C(102)	1.1227(7)	−0.2592(3)	0.7356(3)	6.5(4)
C(103)	1.0242(8)	−0.2455(5)	0.7410(4)	7.5(5)
C(104)	0.9748(6)	−0.2852(5)	0.7798(4)	7.6(5)
C(105)	1.0210(6)	−0.3368(4)	0.8156(4)	6.5(4)
C(106)	1.1209(5)	−0.3480(3)	0.8066(3)	4.4(3)
C(200)	0.1416(7)	0.1904(6)	0.0748(5)	11.6(7)
C(201)	0.2393(5)	0.2066(4)	0.0567(4)	6.1(4)
C(202)	0.3130(6)	0.2234(5)	0.0952(4)	7.1(5)
C(203)	0.4071(8)	0.2368(5)	0.0849(4)	8.5(6)
C(204)	0.4245(7)	0.2334(5)	0.0269(5)	8.3(6)
C(205)	0.3581(8)	0.2172(5)	−0.0168(4)	7.4(5)
C(206)	0.2604(7)	0.2023(5)	−0.0004(4)	7.7(5)
C(207)	0.600(1)	−0.0325(9)	0.9261(7)	16.9(6)
C(208)	0.552(1)	−0.016(1)	0.9658(9)	19.8(7)
C(209)	0.487(2)	0.0263(9)	0.993(1)	7.9(5)

[a] Numbers in parentheses are estimated standard deviations of the last significant figure. See Figure 4 for atom-labeling scheme. [b] $B(\text{eq}) = {}^4/_3[a^2\beta_{11} + b^2\beta_{22} + c^2\beta_{33} + 2ab(\cos\gamma)\beta_{12} + 2ac(\cos\beta)\beta_{13} + 2bc(\cos\alpha)\beta_{23}]$.

Table 4. Final Positional Parameters and B(eq) Values for [Cp*Ta(OH_2)(*p-tert*-butylcalix[4]arene)]·acetone, **2b**·acetone[a]

atom	x	y	z	B(eq)[b] (Å^2)
Ta	0.07787(2)	0.721543(8)	0.572945(8)	1.110(8)
O(1)	0.1706(3)	0.7358(1)	0.4831(1)	1.4(1)
O(20)	0.2032(2)	0.6552(1)	0.5765(1)	1.3(1)
O(40)	0.2019(3)	0.7838(1)	0.5999(1)	1.5(1)
O(60)	−0.0131(3)	0.7928(1)	0.5360(1)	1.3(1)
O(80)	−0.0135(2)	0.6655(1)	0.5138(1)	1.3(1)
O(100)	0.7650(5)	0.1900(2)	0.6114(2)	6.2(3)
C(1)	0.0504(4)	0.6596(2)	0.6755(2)	1.9(2)
C(2)	0.0739(4)	0.7236(3)	0.6926(2)	2.0(2)
C(3)	−0.0215(4)	0.7608(2)	0.6685(2)	1.7(2)
C(4)	−0.1042(4)	0.7206(2)	0.6371(2)	1.8(2)
C(5)	−0.0595(4)	0.6583(2)	0.6418(2)	2.0(2)
C(6)	0.1250(5)	0.6037(3)	0.6937(3)	3.5(3)
C(7)	0.1787(5)	0.7448(3)	0.7325(3)	3.5(3)
C(8)	−0.0359(6)	0.8305(3)	0.6772(3)	3.7(3)
C(9)	−0.2219(5)	0.7399(3)	0.6075(3)	3.5(3)
C(10)	−0.1230(6)	0.6000(3)	0.6187(3)	3.5(3)
C(20)	0.2913(4)	0.6376(2)	0.5367(2)	1.3(2)
C(21)	0.2686(4)	0.5921(2)	0.4896(2)	1.3(2)
C(22)	0.3629(4)	0.5736(2)	0.4513(2)	1.4(2)
C(23)	0.4785(4)	0.5990(2)	0.4579(2)	1.5(2)
C(24)	0.4954(4)	0.6456(2)	0.5038(2)	1.6(2)
C(25)	0.4045(4)	0.6661(2)	0.5433(2)	1.3(2)
C(26)	0.4258(4)	0.7190(2)	0.5901(2)	1.7(2)
C(27)	0.5820(4)	0.5780(2)	0.4153(2)	1.8(2)
C(28)	0.5619(5)	0.5111(3)	0.3890(2)	2.9(2)
C(29)	0.7008(4)	0.5770(3)	0.4533(3)	2.5(2)
C(30)	0.5944(5)	0.6247(3)	0.3601(3)	4.0(3)
C(40)	0.2889(4)	0.8129(2)	0.5657(2)	1.3(2)
C(41)	0.4010(4)	0.7836(2)	0.5604(2)	1.5(2)
C(42)	0.4877(4)	0.8129(2)	0.5244(2)	1.7(2)
C(43)	0.4678(4)	0.8692(2)	0.4918(2)	1.8(2)
C(44)	0.3556(4)	0.8973(2)	0.4981(2)	1.7(2)
C(45)	0.2654(4)	0.8700(2)	0.5342(2)	1.4(2)
C(46)	0.1420(4)	0.9007(2)	0.5363(2)	1.6(2)
C(47)	0.5658(4)	0.8960(2)	0.4496(3)	2.3(2)
C(48)	0.6792(5)	0.9095(3)	0.4896(3)	3.1(3)
C(49)	0.5271(5)	0.9560(3)	0.4149(3)	3.3(3)
C(50)	0.5952(5)	0.8469(3)	0.3981(3)	3.5(3)
C(60)	−0.0076(4)	0.8271(2)	0.4812(2)	1.4(2)
C(61)	0.0611(4)	0.8824(2)	0.4804(2)	1.6(2)
C(62)	0.0587(4)	0.9187(2)	0.4251(2)	1.7(2)
C(63)	−0.0061(4)	0.9017(2)	0.3704(2)	1.9(2)
C(64)	−0.0697(4)	0.8447(2)	0.3728(2)	1.6(2)
C(65)	−0.0711(4)	0.8073(2)	0.4265(2)	1.4(2)
C(66)	−0.1401(4)	0.7448(2)	0.4257(2)	1.4(2)
C(67)	−0.0113(5)	0.9417(2)	0.3097(2)	2.4(2)
C(68)	0.0898(6)	0.9907(3)	0.3088(3)	4.4(3)
C(69)	−0.1316(5)	0.9769(3)	0.3069(3)	3.5(3)
C(70)	−0.0009(6)	0.9003(3)	0.2501(3)	3.7(3)
C(80)	−0.0040(4)	0.6520(2)	0.4512(2)	1.2(2)
C(81)	−0.0653(4)	0.6888(2)	0.4053(2)	1.3(2)
C(82)	−0.0569(4)	0.6733(2)	0.3413(2)	1.5(2)
C(83)	0.0123(4)	0.6221(2)	0.3203(2)	1.8(2)
C(84)	0.0741(4)	0.5884(2)	0.3669(2)	1.6(2)
C(85)	0.0691(4)	0.6019(2)	0.4318(2)	1.3(2)
C(86)	0.1442(4)	0.5647(2)	0.4794(2)	1.3(2)
C(87)	0.0163(5)	0.6072(3)	0.2488(2)	2.4(2)
C(88)	−0.1082(5)	0.5864(3)	0.2246(3)	4.0(3)
C(89)	0.1045(6)	0.5555(3)	0.2340(3)	4.1(3)
C(90)	0.0535(6)	0.6665(3)	0.2115(3)	4.4(3)
C(91)	0.7189(5)	0.2153(3)	0.6565(3)	3.1(3)
C(92)	0.686(1)	0.2828(4)	0.6533(4)	6.9(5)
C(93)	0.6880(6)	0.1777(4)	0.7129(3)	4.7(3)
H(1)	0.1468	0.7513	0.4506	2.1
H(2)	0.2347	0.7186	0.4784	2.1

[a] Numbers in parentheses are estimated standard deviations of the last significant figure. See Figure 9 for atom-labeling scheme. [b] B(eq) = $4/3[a^2\beta_{11} + b^2\beta_{22} + c^2\beta_{33} + 2ab(\cos\gamma)\beta_{12} + 2ac(\cos\beta)\beta_{13} + 2bc(\cos\alpha)\beta_{23}]$.

Basis functions were generated according to Herman and Skillman's numerical Xα atomic orbital program[25] and used with Bursten and Fenske's Xα-to-STO modifications.[26,27] The molecular z axis is located along the Cp*Ta−calix vector with the origin taken at the tantalum atom. For each atom a local coordinate system was defined, with positive z axis pointing toward Ta and a component of the y axis in the negative z direction of the molecular coordinate system such that the local x axis lies in the molecular xy plane. Calculations were performed for [Cp*Ta]$^{4-}$, [calix[4]arene]$^{4-}$, [Cp*Ta(calix[4]arene)] (**1**), [Cp*Ta(calix[4]arene-C_{4v})], [Cp*Ta(OH_2)(calix[4]arene)], and [Cp*Ta($NCCH_3$)(calix[4]arene)]. The last two complexes serve as models for **2b** and **2c**, respectively. Geometric parameters for each Ta center and bonded main group atoms were taken from X-ray crystallographic studies with the exception of those for [Cp*Ta(calix[4]arene-C_{4v})], for which idealized C_{4v} symmetry was assigned to the calixarene ligand.

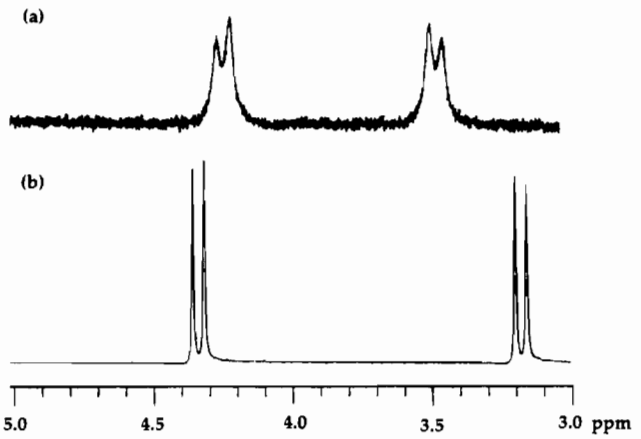

Figure 2. Methylene regions of the ^{1}H NMR spectra of (a) free *p-tert*-butylcalix[4]arene and (b) [Cp*Ta(*p-tert*-butylcalix[4]arene)], **2a**.

^{2}H NMR Spectral Study of [Cp*Ta($NCCD_3$)(*p-tert*-butylcalix[4]-arene)] (2c-*d*$_3$). Crystals of **2c-*d*$_3$**·2.5CH_2Cl_2 were grown by cooling a solution of **2a** in CH_2Cl_2/$NCCD_3$ to −30 °C. The crystals were crushed and dried in vacuo overnight, removing the methylene chloride of crystallization. To a solution of the resulting powder (50 mg, 0.050 mmol) dissolved in 2 mL of CH_2Cl_2 in an NMR tube was added an extra 1 equiv of $NCCD_3$ (2.5 μL) by syringe. Spectra were collected on a Varian XL300 spectrometer with a multinuclear probe and externally referenced to C_6D_6 in benzene. Temperatures were calibrated by using pure methanol. Sweep widths of 6500 Hz were scanned for features before focusing on the observed peaks.

Results and Discussion

Syntheses of [Cp*Ta(calix[4]arene)] (1), [Cp*Ta(*p-tert*-butylcalix[4]arene)] (2a), and [CpNb(*p-tert*-butylcalix[4]-arene)] (3). Transition metal calixarene complexes **1**, **2a**, and **3** were prepared by two routes, from the protonated or deprotonated ligand. In the former method, the (pentamethylcyclopentadienyl)- or (cyclopentadienyl)metal tetrachloride was allowed to react with the calixarene macrocycle over approximately 2 days in refluxing toluene. The reactions were easily monitored by following the evolution of HCl gas and produced very good yields of the desired products. With some loss in yield, preparation from the anionic ligands gave the desired products in less time. In the latter procedure, the calixarene macrocycles were first deprotonated and then allowed to react in situ with the (pentamethylcyclopentadienyl)- or (cyclopentadienyl)metal tetrachloride. Residual calixarene or transition metal starting materials were removed when necessary by extracting the products into nonpolar solvents and passing a solution of the crude mixture through alumina. All of the products were hygroscopic but otherwise very stable and soluble in a variety of polar and nonpolar solvents.

(24) Hall, M. B.; Fenske, R. F. *Inorg. Chem.* **1972**, *11*, 768.
(25) Herman, F.; Skillman, S. *Atomic Structure Calculations*; Prentice-Hall: Englewood Cliffs, NJ, 1963.
(26) Bursten, B. E.; Fenske, R. F. *J. Chem. Phys.* **1977**, *67*, 3138.
(27) Bursten, B. E.; Jensen, R. J.; Fenske, R. F. *J. Chem. Phys.* **1978**, *68*, 3320.

Table 5. Final Positional Parameters and B(eq) Values for [Cp*Ta($NCCH_3$)(*p-tert*-butylcalix[4]arene)]·2.5CH_2Cl_2, **2c**·2.5CH_2Cl_2[a]

atom	x	y	z	B(eq)[b] (Å^2)	atom	x	y	z	B(eq)[b] (Å^2)
Ta(100)	0.781233(12)	0.371401(10)	0.801458(17)	1.412(8)	C(181)	0.68501(29)	0.33650(24)	1.03891(38)	1.5(2)
Ta(200)	0.225230(12)	0.074531(10)	0.598654(17)	1.498(8)	C(182)	0.66159(29)	0.35533(26)	1.12541(41)	1.8(2)
Cl(1)	0.91349(22)	0.16227(16)	0.68620(28)	11.2(2)	C(183)	0.70472(30)	0.40405(26)	1.20020(42)	1.8(2)
Cl(2)	0.97051(17)	0.25169(15)	0.55408(30)	10.3(2)	C(184)	0.77285(30)	0.43449(26)	1.18257(41)	1.8(2)
Cl(3)	0.96180(12)	0.41488(11)	0.31949(17)	5.5(1)	C(185)	0.79848(28)	0.41856(25)	1.09668(41)	1.5(2)
Cl(4)	0.98308(12)	0.30415(10)	0.22093(21)	6.1(1)	C(186)	0.87098(30)	0.45817(26)	1.07709(43)	2.0(2)
Cl(5)	0.54261(16)	0.13282(12)	0.50603(24)	8.1(1)	C(187)	0.68002(34)	0.42304(30)	1.29803(46)	2.6(2)
Cl(6)	0.51302(13)	0.23982(11)	0.43252(16)	6.2(1)	C(188)	0.72538(47)	0.41050(43)	1.38959(53)	5.3(4)
Cl(7)	0.16638(17)	0.16878(15)	0.17563(23)	8.8(1)	C(189)	0.69105(54)	0.49317(42)	1.30970(66)	6.1(4)
Cl(8)	0.09103(16)	0.22199(13)	0.30474(24)	8.3(1)	C(190)	0.60403(46)	0.38867(49)	1.30043(65)	7.0(4)
Cl(9)	0.15195(18)	0.35643(14)	0.53835(28)	9.7(2)	C(201)	0.20866(32)	0.16666(27)	0.51579(42)	2.0(2)
Cl(10)	0.08210(14)	0.44346(14)	0.59513(21)	7.9(1)	C(202)	0.14140(32)	0.12111(28)	0.51019(42)	2.1(2)
O(120)	0.86115(19)	0.44935(16)	0.86121(27)	1.7(1)	C(203)	0.13910(31)	0.06620(27)	0.44698(42)	2.1(2)
O(140)	0.76209(19)	0.41585(17)	0.68603(27)	1.7(1)	C(204)	0.20524(31)	0.07802(27)	0.41476(41)	2.0(2)
O(160)	0.67941(19)	0.31541(16)	0.76533(27)	1.7(1)	C(205)	0.24894(32)	0.14033(28)	0.45668(43)	2.2(2)
O(180)	0.77804(19)	0.34920(16)	0.94067(26)	1.6(1)	C(206)	0.23195(35)	0.23173(28)	0.57109(48)	2.9(2)
O(220)	0.26170(19)	0.14874(17)	0.70500(27)	1.8(1)	C(207)	0.08151(35)	0.13066(31)	0.55795(50)	3.1(3)
O(240)	0.14034(20)	0.04613(17)	0.66550(28)	2.0(1)	C(208)	0.07528(35)	0.00767(30)	0.41489(48)	3.0(2)
O(260)	0.20373(20)	−0.01545(16)	0.54210(27)	1.8(1)	C(209)	0.22594(36)	0.03535(30)	0.34252(45)	2.9(2)
O(280)	0.32459(19)	0.08738(16)	0.58153(26)	1.6(1)	C(210)	0.32185(35)	0.17337(30)	0.43791(48)	2.9(2)
N(10)	0.72552(23)	0.43269(20)	0.86748(33)	1.5(2)	C(220)	0.29370(30)	0.16022(24)	0.80301(40)	1.7(2)
N(20)	0.26567(24)	0.03643(20)	0.73370(34)	1.6(2)	C(221)	0.36771(29)	0.17735(23)	0.82564(40)	1.5(2)
C(10)	0.69979(30)	0.46327(27)	0.90465(46)	2.1(2)	C(222)	0.39973(29)	0.18622(25)	0.92742(42)	1.7(2)
C(11)	0.66843(43)	0.50551(41)	0.95356(84)	7.3(4)	C(223)	0.36070(31)	0.17791(25)	1.00750(42)	1.9(2)
C(20)	0.28921(31)	0.02027(26)	0.80242(43)	2.0(2)	C(224)	0.28731(32)	0.16128(26)	0.98138(43)	2.0(2)
C(21)	0.31945(48)	−0.00045(39)	0.89197(57)	5.3(4)	C(225)	0.25287(29)	0.15159(24)	0.88097(41)	1.6(2)
C(101)	0.89351(30)	0.35287(28)	0.76625(45)	2.2(2)	C(226)	0.17223(31)	0.12758(28)	0.85609(43)	2.1(2)
C(102)	0.85896(36)	0.30519(31)	0.82119(47)	2.8(2)	C(227)	0.39567(33)	0.18712(28)	1.11891(43)	2.3(2)
C(103)	0.79497(34)	0.26838(28)	0.75961(54)	2.8(2)	C(228)	0.38785(43)	0.24573(33)	1.17586(47)	3.9(3)
C(104)	0.78891(32)	0.29366(28)	0.66676(46)	2.3(2)	C(229)	0.35943(36)	0.12997(32)	1.17020(47)	3.2(3)
C(105)	0.85001(30)	0.34590(26)	0.67139(42)	1.9(2)	C(230)	0.47404(37)	0.19514(36)	1.13048(48)	3.8(3)
C(106)	0.96469(34)	0.40197(36)	0.79914(57)	4.1(3)	C(240)	0.12750(28)	0.01949(26)	0.75096(43)	1.9(2)
C(107)	0.88792(46)	0.29291(43)	0.92407(55)	5.2(4)	C(241)	0.14069(29)	0.05693(27)	0.84540(44)	2.0(2)
C(108)	0.74307(44)	0.20984(33)	0.78583(74)	5.6(4)	C(242)	0.12770(32)	0.02745(29)	0.93138(44)	2.5(2)
C(109)	0.72936(37)	0.26589(36)	0.57813(56)	4.2(3)	C(243)	0.10303(32)	−0.03716(29)	0.92924(46)	2.5(2)
C(110)	0.86828(38)	0.38443(34)	0.58711(51)	3.5(3)	C(244)	0.09131(30)	−0.07256(28)	0.83376(45)	2.3(2)
C(120)	0.86375(28)	0.50469(25)	0.91250(43)	1.7(2)	C(245)	0.10314(29)	−0.04659(27)	0.74452(42)	1.9(2)
C(121)	0.86824(28)	0.51202(26)	1.01858(42)	1.7(2)	C(246)	0.09620(30)	−0.08788(27)	0.64557(45)	2.2(2)
C(122)	0.86498(29)	0.56706(27)	1.06829(43)	2.1(2)	C(247)	0.09498(39)	−0.06740(34)	1.02669(51)	3.7(3)
C(123)	0.86000(30)	0.61679(27)	1.01655(47)	2.3(2)	C(248)	0.06879(50)	−0.03061(49)	1.10444(63)	6.4(4)
C(124)	0.85848(30)	0.60867(25)	0.91207(46)	2.0(2)	C(249)	0.04545(77)	−0.13515(50)	1.00575(70)	13.6(6)
C(125)	0.85945(29)	0.55407(27)	0.85759(44)	2.0(2)	C(250)	0.16697(54)	−0.06746(45)	1.07655(63)	6.1(4)
C(126)	0.85016(31)	0.54525(26)	0.74239(44)	2.1(2)	C(260)	0.21599(30)	−0.06407(24)	0.58710(40)	1.8(2)
C(127)	0.85596(35)	0.67807(30)	1.07213(52)	3.0(2)	C(261)	0.16413(32)	−0.10146(25)	0.63729(42)	2.0(2)
C(128)	0.91931(53)	0.73233(40)	1.0659(10)	9.6(6)	C(262)	0.17938(32)	−0.14870(26)	0.68674(45)	2.2(2)
C(129)	0.79114(56)	0.69066(46)	1.02128(87)	8.3(5)	C(263)	0.24275(32)	−0.15993(26)	0.68792(45)	2.2(2)
C(130)	0.84794(77)	0.67414(45)	1.18248(81)	9.9(6)	C(264)	0.29177(31)	−0.12294(25)	0.63480(43)	2.0(2)
C(140)	0.73125(30)	0.46052(26)	0.67086(39)	1.7(2)	C(265)	0.27959(30)	−0.07540(25)	0.58396(41)	1.8(2)
C(141)	0.77323(29)	0.52431(26)	0.69284(41)	1.8(2)	C(266)	0.33752(31)	−0.03297(25)	0.53572(41)	1.9(2)
C(142)	0.74013(32)	0.56843(25)	0.67221(42)	2.0(2)	C(267)	0.25822(36)	−0.20989(30)	0.74825(51)	3.0(2)
C(143)	0.66936(33)	0.55268(28)	0.63404(44)	2.3(2)	C(268)	0.20570(40)	−0.27477(31)	0.69993(58)	3.9(3)
C(144)	0.62935(30)	0.48837(28)	0.61536(42)	2.0(2)	C(269)	0.33229(41)	−0.21240(37)	0.74635(69)	5.2(4)
C(145)	0.65865(30)	0.44226(26)	0.63432(40)	1.7(2)	C(270)	0.24815(52)	−0.19808(36)	0.85906(57)	5.4(4)
C(146)	0.61260(29)	0.37381(26)	0.61927(41)	1.8(2)	C(280)	0.38059(29)	0.07669(25)	0.63570(40)	1.6(2)
C(147)	0.63225(36)	0.60123(30)	0.61176(51)	3.0(2)	C(281)	0.39113(30)	0.01926(25)	0.61320(40)	1.7(2)
C(148)	0.60467(55)	0.59279(42)	0.49888(64)	6.4(4)	C(282)	0.44816(31)	0.00920(26)	0.67087(44)	2.0(2)
C(149)	0.57260(43)	0.59320(35)	0.67220(71)	5.1(4)	C(283)	0.49554(30)	0.05381(27)	0.74833(43)	2.0(2)
C(150)	0.68481(42)	0.66874(33)	0.64350(65)	4.5(3)	C(284)	0.48291(30)	0.11067(27)	0.76690(42)	2.0(2)
C(160)	0.61969(28)	0.32597(24)	0.78524(40)	1.5(2)	C(285)	0.42652(29)	0.12254(25)	0.71276(41)	1.7(2)
C(161)	0.58484(29)	0.35406(24)	0.71554(41)	1.7(2)	C(286)	0.41219(28)	0.18341(25)	0.74150(41)	1.7(2)
C(162)	0.52649(29)	0.36832(24)	0.74091(41)	1.7(2)	C(287)	0.55636(33)	0.03895(30)	0.80926(49)	2.6(2)
C(163)	0.50190(29)	0.35712(24)	0.83259(42)	1.7(2)	C(288)	0.60706(38)	0.02925(38)	0.73875(59)	4.4(3)
C(164)	0.53736(28)	0.32936(25)	0.89903(40)	1.7(2)	C(289)	0.59827(37)	0.09078(34)	0.89722(55)	3.8(3)
C(165)	0.59525(27)	0.31254(23)	0.87664(39)	1.3(2)	C(290)	0.52491(39)	−0.02173(33)	0.85588(55)	3.9(3)
C(166)	0.63455(29)	0.28577(25)	0.95593(41)	1.7(2)	C(300)	0.89639(46)	0.20732(42)	0.59545(68)	5.8(4)
C(167)	0.43945(31)	0.37748(27)	0.85730(45)	2.2(2)	C(301)	0.95677(41)	0.37003(37)	0.20360(61)	4.6(3)
C(168)	0.37302(34)	0.34197(32)	0.77866(53)	3.3(3)	C(302)	0.51697(40)	0.19754(35)	0.53562(55)	4.0(3)
C(169)	0.42199(36)	0.36443(33)	0.96232(53)	3.4(3)	C(303)	0.10608(42)	0.15570(38)	0.25708(58)	4.5(3)
C(170)	0.45744(37)	0.44832(31)	0.85321(54)	3.4(3)	C(304)	0.11733(52)	0.41176(47)	0.50135(65)	6.3(4)
C(180)	0.75441(28)	0.36786(25)	1.02428(39)	1.5(2)					

[a] Numbers in parentheses are estimated standard deviations of the last significant figure. See Figure 11 for atom-labeling scheme. [b] $B(\text{eq}) = {}^4/_3[a^2\beta_{11} + b^2\beta_{22} + c^2\beta_{33} + 2ab(\cos\gamma)\beta_{12} + 2ac(\cos\beta)\beta_{13} + 2bc(\cos\alpha)\beta_{23}]$.

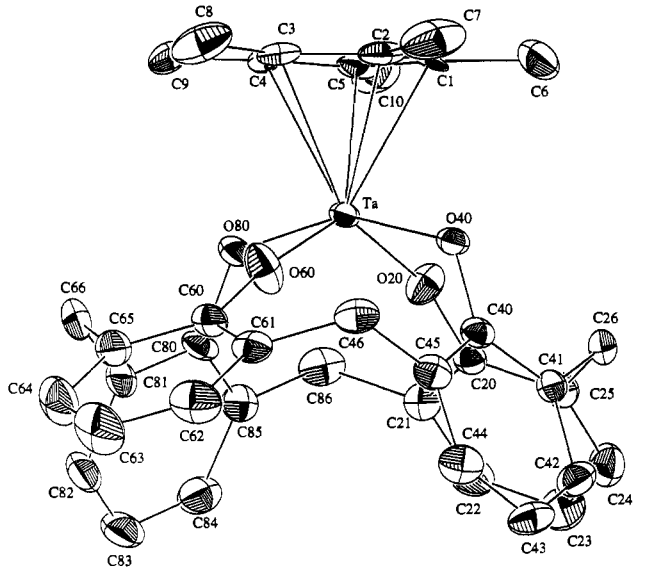

Figure 3. ORTEP diagram of [Cp*Ta(calix[4]arene)], **1**, showing the atom-labeling scheme and 50% probability ellipsoids.

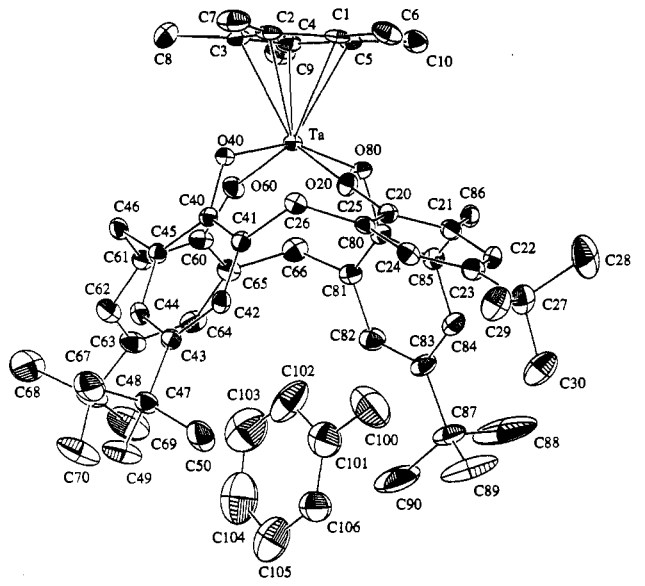

Figure 4. ORTEP drawing of [Cp*Ta(*p-tert*-butylcalix[4]arene)]·toluene, **2a**·toluene, showing the atom-labeling scheme and 40% probability ellipsoids.

The nature of products **1**, **2a**, and **3** was determined by ^{1}H NMR and IR spectroscopy, mass spectrometry, and elemental analysis. Calix[4]arene and *p-tert*-butylcalix[4]arene macrocycles give rise to very characteristic and uncomplicated ^{1}H NMR spectra. In the free ligands, the diastereotopic protons on the methylene groups linking the phenol moieties appear as a pair of broad doublets, due to interconversion of cone conformers.[5a,21] The most obvious sign of calixarene ligand metalation is the dramatic sharpening of this pair of doublets because of the rigid cone conformation imparted to the ligand. This effect is illustrated in Figure 2, which shows the methylene regions in the ^{1}H NMR spectra of the free *p-tert*-butylcalix[4]-arene and of the product [Cp*Ta(*p-tert*-butylcalix[4]arene)] (**2a**), in which the ligand is geometrically constrained. The presence of only one pair of doublets in the ^{1}H NMR spectra of the products **1**, **2a**, and **3** in solution suggested that, as in the free ligands, the calixarene has approximate 4-fold symmetry. Further evidence of metal coordination by the calixarene ligands was provided by the disappearance of the phenol resonance at

Table 6. Selected Interatomic Bond Distances (Å) and Angles (deg) for [Cp*Ta(calix[4]arene)], **1**[a]

	Bond Distances		
Ta−O(20)	1.902(4)	Ta−C(2)	2.447(5)
Ta−O(40)	2.010(3)	Ta−C(3)	2.476(5)
Ta−O(60)	1.871(4)	Ta−C(4)	2.480(5)
Ta−O(80)	2.000(3)	Ta−C(5)	2.425(5)
Ta−C(1)	2.424(5)		
	Bond Angles		
O(20)−Ta−O(40)	84.3(1)	O(40)−Ta−O(60)	84.1(1)
O(20)−Ta−O(60)	127.0(2)	O(40)−Ta−O(80)	155.1(1)
O(20)−Ta−O(80)	84.8(1)	O(60)−Ta−O(80)	84.7(1)
Ta−O(20)−C(20)	160.8(4)	Ta−O(60)−C(60)	171.6(4)
Ta−O(40)−C(40)	124.1(3)	Ta−O(80)−C(80)	125.2(3)

[a] Estimated standard deviations in the least significant figure are given in parentheses.

Table 7. Selected Interatomic Bond Distances (Å) and Angles (deg) for [Cp*Ta(*p-tert*-butylcalix[4]arene)]·toluene, **2a**·toluene[a]

	Bond Distances		
Ta−O(20)	1.879(3)	Ta-C(2)	2.450(4)
Ta−O(40)	2.002(3)	Ta-C(3)	2.429(4)
Ta−O(60)	1.893(3)	Ta-C(4)	2.437(4)
Ta−O(80)	1.999(3)	Ta-C(5)	2.473(4)
Ta-C(1)	2.451(4)		
	Bond Angles		
O(20)−Ta−O(40)	83.0(1)	O(40)−Ta−O(60)	84.9(1)
O(20)−Ta−O(60)	123.6(1)	O(40)−Ta−O(80)	155.2(1)
O(20)−Ta−O(80)	83.5(1)	O(60)−Ta−O(80)	85.3(1)
Ta−O(20)−C(20)	178.4(3)	Ta−O(60)−C(60)	158.4(3)
Ta−O(40)−C(40)	124.2(2)	Ta−O(80)−C(80)	123.3(2)

[a] Estimated standard deviations in the least significant figure are given in parentheses.

ca. 9−10 ppm present in the ^{1}H NMR spectra of the free ligands with the concomitant appearance of resonances at *ca.* 2.5 or 7.1 ppm. These resonances are assigned respectively to pentamethylcyclopentadienyl or cyclopentadienyl ligands. The IR spectra of the products **1**, **2a**, and **3** were also informative when compared with those of the free ligands, revealing the disappearance of the broad band arising from the PhO−H stretch of the free ligand and the appearance of a new band in the 750−850 cm^{-1} region, assignable to M−O stretch (M = Ta, Nb).[28] Mass spectrometry and elemental analyses further supported the assignments of **1**, **2a**, and **3**.

Structures of [Cp*Ta(calix[4]arene)] (1) and [Cp*Ta(*p-tert*-butylcalix[4]arene)]·2toluene·pentane (2a·2toluene·pentane). Single-crystal X-ray analyses revealed the nature of products **1** and **2a** in the solid state, and their structures are shown in Figures 3 and 4, respectively. Selected bond distances and angles for **1** and **2a**·2toluene·pentane are given in Tables 6 and 7, respectively. Both complexes contain a Cp*Ta moiety mounted onto the tetraphenoxide rim of a calixarene at the top of the macrocyclic pocket. In the solid state these products are distorted from the 4-fold symmetry of the free ligands, producing elliptical rather than circular calixarene cavities. This shape can be seen by looking down the vector containing the centroid of the Cp* ring and the Ta atom as shown for both **1** and **2a**·2toluene·pentane in Figure 5 and by analysis of the metrical parameters. There is approximately a 30° difference in the *endo*-calix angles O(20)−Ta−O(60) and O(40)−Ta−O(80) for both **1** and **2a**·2toluene·pentane. The Ta−O_{calix} distances for both complexes also vary, with the average Ta−O(20) and Ta−O(60) bond distance in [Cp*Ta(calix[4]arene)] (**1**) of 1.89(2) Å being

(28) Nakamoto, K. *Infrared and Raman Spectra of Inorganic and Coordination Compounds*, 3rd ed.; Wiley-Interscience: New York, 1977.

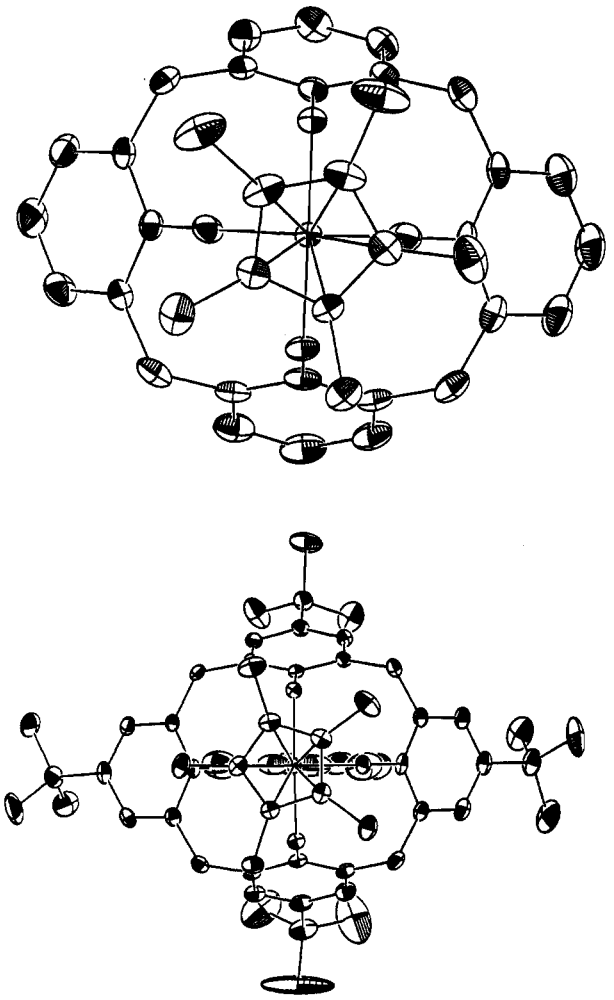

Figure 5. Top views of ORTEP diagrams of [Cp*Ta(calix[4]arene)], **1**, and [Cp*Ta(*p-tert*-butylcalix[4]arene)]·toluene, **2a**·toluene.

significantly shorter than the Ta−O(40) and Ta−O(80) average bond length of 2.005(5) Å. It is instructive to compare these distances with those previously reported for compounds containing Ta−O bonds. A survey of 45 compounds in the Cambridge Structural Database containing 100 Ta−O−C bonds shows an average Ta−O bond length of 1.90(4) Å.[29] Crystallographically characterized Ta−O bonds of higher order are rare but include the Ta=O distance of 1.70(2) Å in $Cp^*_2Ta(=O)H$.[30] The Ta−O_{calix} distances reported here are therefore effectively single bonds. The difference between the Ta−O(20), Ta−O(60) and Ta−O(40), Ta−O(80) distances suggests different oxygen−metal π interactions, however, as discussed below.

The Ta−O−C_{calix} angles range from ca. 124° to almost linear, and the trans angles Ta−O(20)−C(20) and Ta−O(60)−C(60) are 34−55° larger than Ta−O(40)−C(40) and Ta−O(80)−C(80). The bending of the calixarene macrocycles in **1** and **2a** can be understood in part by considering that both contain d^0 Ta(V) metal centers and are formally 14 e complexes. The phenoxide groups of the calixarenes are capable of donating π as well as σ electrons, the relative contributions of which are reflected in the shortening of the Ta−O distances and a related increase in the Ta−O−Ph bend angles.[31] An approximately linear relationship can be seen in a plot of Ta−O_{calix} distances

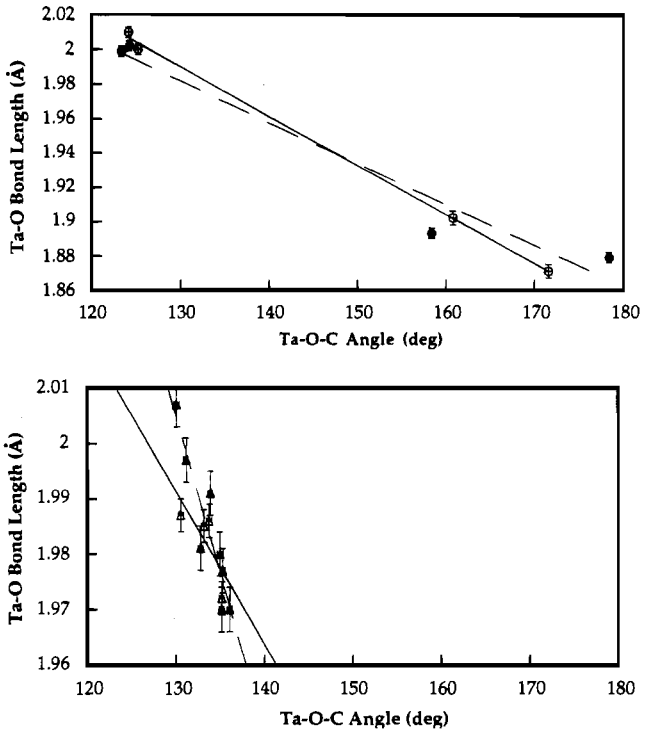

Figure 6. Plots of the Ta−O−C_{calix} angles versus Ta−O_{calix} bond lengths: [Cp*Ta(calix[4]arene)] (**1**) (open circles) and [Cp*Ta(*p-tert*-butylcalix[4]arene)] (**2a**) (filled circles) in the top graph; [Cp*Ta(OH_2)-(*p-tert*-butylcalix[4]arene)] (**2b**) (open triangles) and [Cp*Ta($NCCH_3$)-(*p-tert*-butylcalix[4]arene)] (**2c**) (filled triangles) in the bottom graph. Solid lines represent best least-squares fit to a linear relationship. Error bars denote ±1 esd.

versus Ta−O−C_{calix} angles (Figure 6, top). As will be discussed later, Fenske−Hall calculations support the prediction that π electron donation from the phenoxide oxygen atoms O(20) and O(60) helps to relieve the electron deficiency at the metal centers in **1** and **2a**. This interaction distorts the products from 4-fold to 2-fold symmetry in the solid state. The distortion is more pronounced in **2a**·2toluene·pentane than in **1**, a difference that can be understood by analysis of intermolecular interactions of these products.

As shown in Figure 4, one of the toluene molecules of **2a**·2toluene·pentane is included sideways in the calixarene pocket. This inclusion can be seen more readily in the packing diagram shown in Figure 7. Such inclusion of aromatic rings by calixarene macrocycles has precedent[6,16,32,33] in the literature. Two types of alkyl−phenyl group interactions are possible between [Cp*Ta(*p-tert*-butylcalix[4]arene)] (**2a**) and the included toluene molecule, those involving the methyl group of the toluene molecule and the phenyl rings of the calixarene and interactions between the *tert*-butyl methyl groups of the calixarene and the π system of the toluene molecule. In the case of **2a**·2toluene·pentane, the methyl group C(100) of the toluene molecule is pointed directly toward the center of the phenyl ring C(20)−C(25) at a distance of 3.59 Å from the plane of the aromatic ring. This distance is similar to that found in other calixarene complexes.[16,20,34] The surprising aspect of the

(29) Allen, F. H.; Davies, J. E.; Galloy, J. J.; Johnson, O.; Kennard, O.; Macrae, C. F.; Mitchell, E. M.; Mitchell, G. F.; Smith, J. M.; Watson, D. G. *J. Chem. Inf. Comput. Sci.* **1991**, *31*, 187.
(30) Parkin, G.; van Asselt, A.; Leahy, D. J.; Whinnery, L.; Hua, N. G.; Quan, R. W.; Henling, L. M.; Schaefer, W. P.; Santarsiero, B. D.; Bercaw, J. E. *Inorg. Chem.* **1992**, *31*, 82.
(31) Chisholm, M. H.; Rothwell, I. P. In *Comprehensive Coordination Chemistry*; Wilkinson, G., Ed.; Pergamon Books: New York, 1987; Vol. 2 (Ligands).
(32) Bott, S. G.; Coleman, A. W.; Atwood, J. L. *J. Am. Chem. Soc.* **1986**, *108*, 1709.
(33) Coruzzi, M.; Andreetti, G. D.; Bocchi, V.; Pochini, A.; Ungaro, R. *J. Chem. Soc., Perkin Trans. 2* **1982**, 1133.
(34) McKervey, M. A.; Seward, E. M.; Ferguson, G.; Ruhl, B. L. *J. Org. Chem.* **1986**, *51*, 3581.

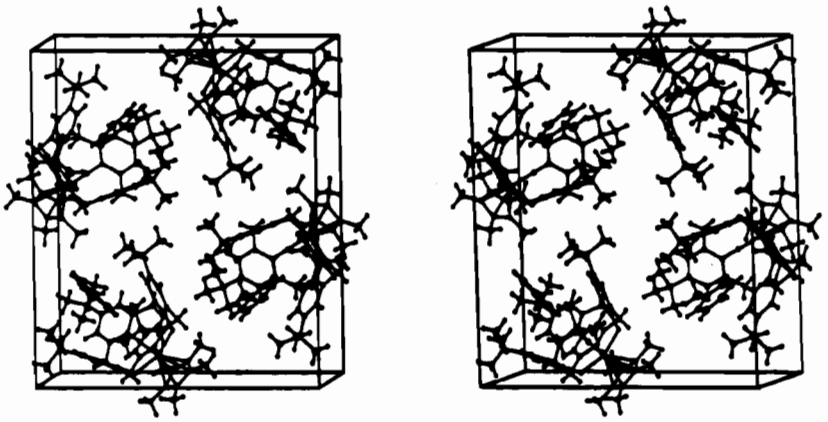

Figure 7. Stereoview packing diagram of [Cp*Ta(*p-tert*-butylcalix[4]arene)]·toluene (**2a**·toluene). Toluene and pentane molecules in the lattice were omitted for clarity.

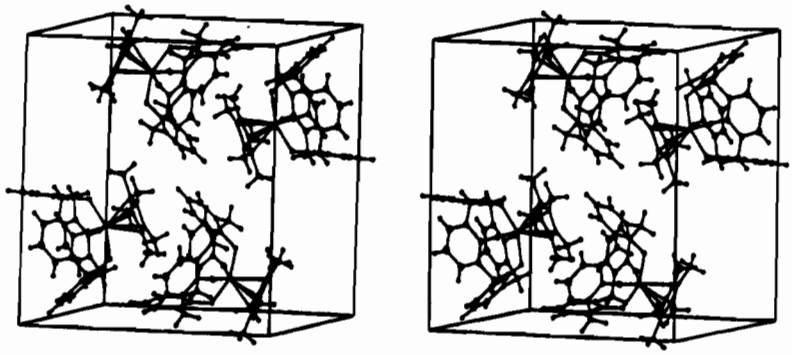

Figure 8. Stereoview packing diagram of [Cp*Ta(calix[4]arene)] (**1**).

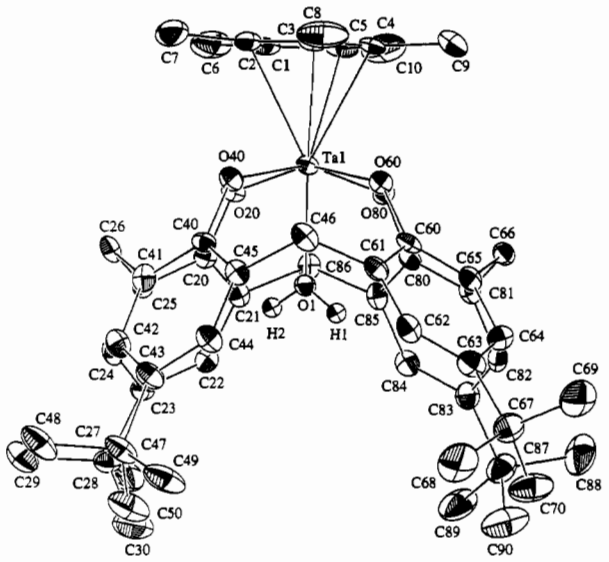

Figure 9. ORTEP drawing of [Cp*Ta(OH_2)(*p-tert*-butylcalix[4]arene)] (**2b**) showing 50% probability ellipsoids and the atom-labeling scheme.

included toluene molecule in **2a**·2toluene·pentane, however, is its sideways orientation (see **I**). Toluene molecules have previously been found to orient with their methyl group pointed up into the calixarene cone (**II**), as seen in the solid state structures of *p-tert*-butylcalix[4]arene·toluene[16] and [(Ti{*p-tert*-butylcalix[4]arene})$_2$]·toluene.[6] The sideways inclusion of toluene by the calixarene ligand in **2a** may have been effected by the elliptical distortion of the *p-tert*-butylcalix[4]arene induced upon binding of the Cp*Ta moiety to the tetraphenoxide rim of the basket. Moreover, the shape of **2a** is further distorted by allowing for sideways inclusion of the toluene molecule in the calixarene pocket, reflected in the Ta−O(20)−C(20) angle of 178.4 (3)° versus the Ta−O(60)−C(60) angle of 158.4 (3)°.

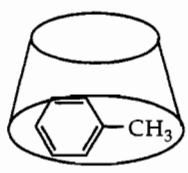

I

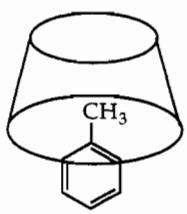

II

Although single crystals of **1** were also grown from a toluene solution, there were no solvent molecules included in the calixarene pocket in its solid state structure. The only difference between **1** and **2a** is the absence of *tert*-butyl groups in **1**. Whereas the methyl groups of the *tert*-butyl moieties of *p-tert*-butylcalix[4]arene may contribute to the alkyl−phenyl interactions in **2a**·2toluene·pentane, these sterically demanding residues would also be expected to inhibit the *endo*-calix interaction of larger guests. In fact, intermolecular interactions do occur in the extended lattice of **1**, as shown in the packing diagram in Figure 8. The methyl groups C(6) and C(7) of the Cp* moiety of [Cp*Ta(calix[4]arene)] (**1**) enter the calixarene pocket of the neighboring molecule. *Endo*-calix interactions ranging from 3.49 to 3.81 Å occur between C(6) and the carbon atoms of the phenyl ring C(20)−C(25) and between C(7) and the carbon atoms of the phenyl ring C(60)−C(65).

Preparation and Structural Characterization of [Cp*Ta(OH_2)(*p-tert*-butylcalix[4]arene)] (2b) and [Cp*Ta($NCCH_3$)(*p-tert*-butylcalix[4]arene)] (2c). If the metal center of [Cp*Ta(*p-tert*-butylcalix[4]arene)] (**2a**) is considered to have approximate C_{4v} symmetry in solution, two of the three metal orbitals of A_1

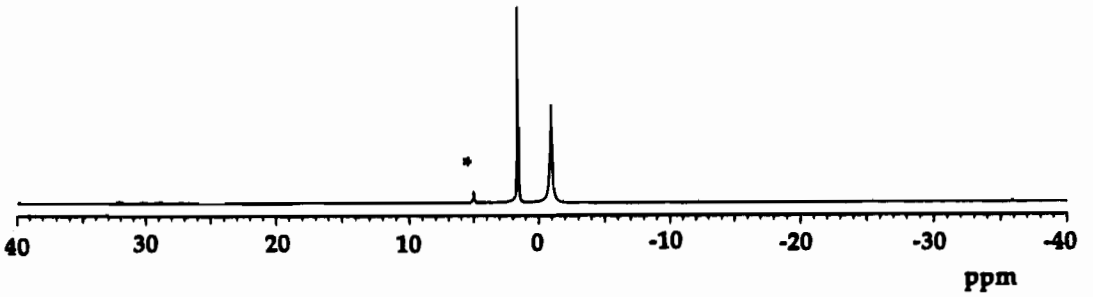

Figure 10. ^2H NMR (CH_2Cl_2) spectrum of [Cp*Ta($NCCD_3$)(*p-tert*-butylcalix[4]arene)] (**2cd_3**) in the presence of excess CD_3CN at −56 °C. The peak labeled with an asterisk arises from CD_2Cl_2.

Table 8. Selected Interatomic Bond Distances (Å) and Angles (deg) for [Cp*Ta(OH_2)(*p-tert*-butylcalix[4]arene)]·acetone, **2b**·acetone[a]

	Bond Distances		
Ta−O(1)	2.188(3)	Ta−C(1)	2.543(5)
Ta−O(20)	1.986(3)	Ta−C(2)	2.509(5)
Ta−O(40)	1.987(3)	Ta−C(3)	2.455(4)
Ta−O(60)	1.972(3)	Ta−C(4)	2.461(4)
Ta−O(80)	1.985(3)	Ta−C(5)	2.516(5)
	Bond Angles		
O(20)−Ta(1)−O(40)	88.5(1)	O(40)−Ta(1)−O(60)	87.3(1)
O(20)−Ta(1)−O(60)	156.3(1)	O(40)−Ta(1)−O(80)	157.2(1)
O(20)−Ta(1)−O(80)	87.2(1)	O(60)−Ta(1)−O(80)	87.7(1)
Ta(1)−O(20)−C(20)	133.8(3)	Ta(1)−O(60)−C(60)	135.2(3)
Ta(1)−O(40)−C(40)	130.6(3)	Ta(1)−O(80)−C(80)	133.2(3)
O(1)−Ta(1)−O(20)	77.6(1)	O(1)−Ta(1)−O(60)	78.7(1)
O(1)−Ta(1)−O(40)	79.2(1)	O(1)−Ta(1)−O(80)	78.0(1)

[a] Estimated standard deviations in the least significant figure are given in parentheses.

symmetry (s, p_z, and d_{z^2}) are predicted[35] to be involved in σ bonding to the calixarene ligand, leaving one orbital available for binding in the *endo*-calix site. This simple analysis was supported by Fenske−Hall calculations, as will be discussed below. Accordingly, when exposed to the small-molecule nucleophiles H_2O and $NCCH_3$, **2a** formed the complexes [Cp*Ta(OH_2)(*p-tert*-butylcalix[4]arene)] (**2b**) and [Cp*Ta($NCCH_3$)(*p-tert*-butylcalix[4]arene)] (**2c**), each coordinated through a heteroatom to the tantalum center in the *endo*-calix position.

The bound H_2O molecule of [Cp*Ta(OH_2)(*p-tert*-butylcalix[4]arene)] (**2b**) gives rise to O−H stretches at 3480 and 3425 cm^{-1} in the IR spectrum and a broad resonance at 2.23 ppm in the ^1H NMR spectrum, shifted downfield from the 1.5 ppm resonance of free H_2O in $CDCl_3$. The presence of the bound water molecule was further revealed by the solid state structure determined crystallographically. An ORTEP drawing of **2b** is shown in Figure 9, and selected bond distances and angles are given in Table 8. The Ta−OH_2 distance of 2.188(3) Å in **2b** is significantly shorter than the Mo−OH_2 distance of 2.408(16) Å in [(H_4-*p-tert*-butylcalix[4]arene)(*p-tert*-butylcalix[4]arene)(Mo=O)(H_2O)($PhNO_2$)].[18,19] These results reflect the weakening of a metal−ligand bond when an oxo group is in the trans position[36] as in the latter complex, as well as the relative electron deficiency of the Ta center in **2b** and in the precursor **2a**. The main structural difference between the precursor complex **2a** and the H_2O adduct **2b** is the increased symmetry associated with the *endo*-calix ligation. The *p-tert*-butylcalix[4]arene ligand in **2b** once again has approximately 4-fold symmetry. The *endo*-calix angles O(20)−Ta−O(60) (156.3 (1)°) and O(40)−Ta−O(80) (157.2 (1)°) are similar, as are the Ta−O_{calix} distances (1.972(3)−1.987(3) Å) and Ta−O_{calix}−C_{calix} angles (130.6(3)°−135.2(3)°). These features arise in part from the steric requirements of accommodating water as an *endo*-calix ligand. The rounding of the calixarene pocket, however, also has an electronic origin. The additional electron density donated by the host ligand to the tantalum center partially alleviates the need for PhO → Ta π electron donation, which desymmetrizes the calixarene geometry. Fenske−Hall calculations support this analysis (vide infra).

Similarly, addition of $NCCH_3$ to **2a** afforded [Cp*Ta($NCCH_3$)(*p-tert*-butylcalix[4]arene)] (**2c**). Whereas complexes **1** and **2a** show no infrared absorptions from 1600 to 2900 cm^{-1}, the IR spectrum of crystalline product **2c** exhibited bands at 2302 and 2332 cm^{-1}. The infrared spectrum of free acetonitrile[37] has bands at 2254 and 2293 cm^{-1}, assigned respectively to the C≡N stretching frequency and a combination band. The combination band results from coupling of the symmetric CH_3 deformation and C−C stretching modes, probably enhanced by Fermi resonance. The shift of these bands to higher frequency upon metal complexation observed in **2c** is well precedented in the literature.[36,38,39]

The room-temperature ^1H NMR spectrum of **2c** exhibited a broad resonance at −0.28 ppm arising from the $NCCH_3$ protons, which are shielded from their position in the uncomplexed ligand, 1.9 ppm for $NCCH_3$ dissolved in $CDCl_3$. The breadth of this resonance at room temperature suggested fluxional behavior. In order to slow down the exchange and observe the resonance of the included molecule unobstructed by resonances from other nuclei, for example *tert*-butyl methyl groups, a low-temperature ^2H NMR study of **2c-d_3** was carried out. Two resonances corresponding to free and bound $NCCD_3$ were observed in the deuterium NMR spectrum below 2 °C. The ^2H NMR spectrum of **2c-d_3** in the presence of excess $NCCD_3$ at −56 °C is shown in Figure 10, with resonances at 1.62 and −0.95 ppm corresponding to free and bound $NCCD_3$, respectively. Although binding to a transition metal center might be expected shift the $NCCH_3$ proton resonance downfield, the solid state structure of **2c** revealed probable shielding effects of *endo*-calix binding which are reflected in their upfield chemical shift.

An ORTEP diagram of one of the molecules in the asymmetric unit of **2c**·2.5CH_2Cl_2 is given in Figure 11, and selected bond angles and distances are provided in Table 9. One molecule of $NCCH_3$ is bound to the tantalum center through the nitrogen atom, leaving the methyl group in the center of the calixarene pocket at an average distance of 3.91 Å from the plane of any of the four aromatic rings. The closest *endo*-calix interactions for the methyl carbons C(11) and C(21) of the two

(35) Cotton, F. A. *Chemical Applications of Group Theory*, 3rd ed.; John Wiley and Sons: New York, 1993.
(36) Cotton, F. A.; Lippard, S. J. *Inorg. Chem.* **1966**, *5*, 9.
(37) Venkateswarlu, P. *J. Chem. Phys.* **1951**, *19*, 293.
(38) Kepert, D. L.; Nyholm, R. S. *J. Chem. Soc.* **1965**, 2871.
(39) Chavant, P. C.; Daran, J. C.; Jeannin, Y.; Constant, G.; Morancho, R. *Acta Crystallogr., Sect. B* **1975**, *31*, 1828.

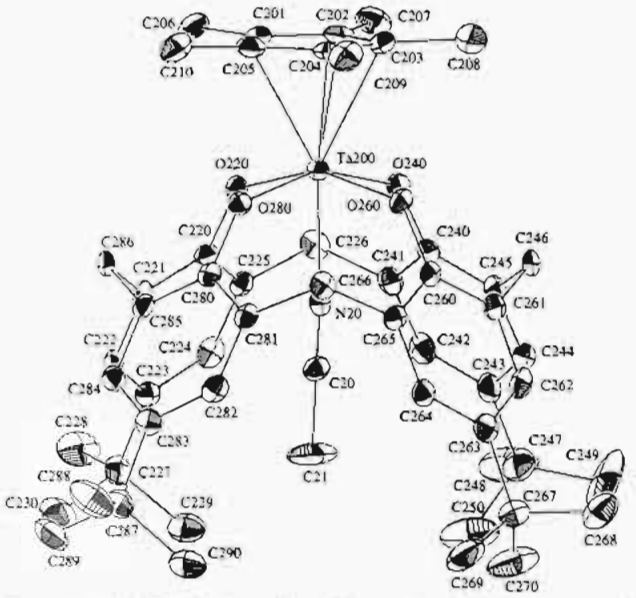

Figure 11. ORTEP drawing of one of the molecules in the asymmetric unit of [Cp*Ta($NCCH_3$)(*p-tert*-butylcalix[4]arene)] (**2c**) showing 40% ellipsoids for non-hydrogen atoms and the atom-labeling scheme. The other molecule contains the atoms Ta(100), N(10), C(10), C(11), O(120), O(140), O(160), O(180), C(120)−C(130), etc.

Table 9. Selected Interatomic Bond Distances (Å) and Angles (deg) for [Cp*Ta($NCCH_3$)(*p-tert*-butylcalix[4]arene)]·2.5CH_2Cl_2, **2c**·2.5CH_2Cl_2[a]

Bond Distances			
Ta(100)−N(10)	2.242(5)	Ta(200)−N(20)	2.237(5)
N(10)−C(10)	1.112(7)	N(20)−C(20)	1.121(7)
C(10)−C(11)	1.461(9)	C(20)−C(21)	1.454(8)
Ta(100)−O(120)	1.988(4)	Ta(200)−O(220)	1.974(4)
Ta(100)−O(140)	1.977(4)	Ta(200)−O(240)	1.989(4)
Ta(100)−O(160)	2.009(4)	Ta(200)−O(260)	2.000(4)
Ta(100)−O(180)	1.972(3)	Ta(200)−O(280)	1.982(4)
Ta(100)−C(101)	2.531(5)	Ta(200)−C(201)	2.522 (7)
Ta(100)−C(102)	2.504(6)	Ta(200)−C(202)	2.494(5)
Ta(100)−C(103)	2.466(6)	Ta(200)−C(203)	2.439(6)
Ta(100)−C(104)	2.460(6)	Ta(200)−C(204)	2.446(5)
Ta(100)−C(105)	2.501(5)	Ta(200)−C(205)	2.517(5)
Bond Angles			
Ta(100)−N(10)−C(10)	176.6(5)	Ta(200)−N(20)−C(20)	176.1(5)
N(10)−C(10)−C(11)	177.8(7)	N(20)−C(20)−C(21)	179.6(7)
O(120)−Ta(100)−O(140)	87.5(1)	O(220)−Ta(200)−O(240)	87.4(1)
O(120)−Ta(100)−O(160)	155.9(1)	O(220)−Ta(200)−O(260)	155.4(1)
O(120)−Ta(100)−O(180)	88.0(1)	O(220)−Ta(200)−O(280)	88.0(1)
O(140)−Ta(100)−O(160)	87.3(1)	O(240)−Ta(200)−O(260)	87.5(2)
O(140)−Ta(100)−O(180)	155.3(1)	O(240)−Ta(200)−O(280)	155.6(1)
O(160)−Ta(100)−O(180)	87.0(1)	O(260)−Ta(200)−O(280)	86.8(1)
Ta(100)−O(120)−C(120)	132.5(3)	Ta(200)−O(220)−C(220)	135.3(3)
Ta(100)−O(140)−C(140)	135.4(3)	Ta(200)−O(240)−C(240)	134.0(3)
Ta(100)−O(160)−C(160)	130.0(3)	Ta(200)−O(260)−C(260)	130.7(3)
Ta(100)−O(180)−C(180)	136.2(3)	Ta(200)−O(280)−C(280)	134.9(3)
O(120)−Ta(100)−N(10)	77.6(1)	O(220)−Ta(200)−N(20)	77.2(2)
O(140)−Ta(100)−N(10)	77.7(1)	O(240)−Ta(200)−N(20)	77.8(2)
O(160)−Ta(100)−N(10)	78.3(1)	O(260)−Ta(200)−N(20)	78.1(1)
O(180)−Ta(100)−N(10)	77.6(1)	O(280)−Ta(200)−N(20)	77.8(1)

[a] Estimated standard deviations in the least significant figure are given in parentheses.

molecules in the asymmetric unit of **2c**·2.5CH_2Cl_2 occur with phenyl carbons C(123) and C(223), respectively, at distances of 3.83 and 3.98 Å. In this position, the methyl group protons are shielded by the four aromatic rings, as evidenced experimentally in solution by the ^1H NMR spectrum.

The Ta−N distances are 2.246 (5) Å for Ta(100)−N(10) and 2.236 (5) Å for Ta(200)−N(20). The distances and angles

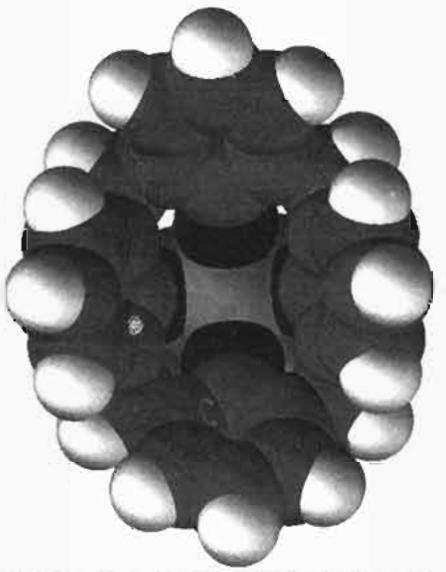

Figure 12. Space-filling diagram of [Cp*Ta(calix[4]arene)] (**1**), viewed into the empty calixarene pocket.

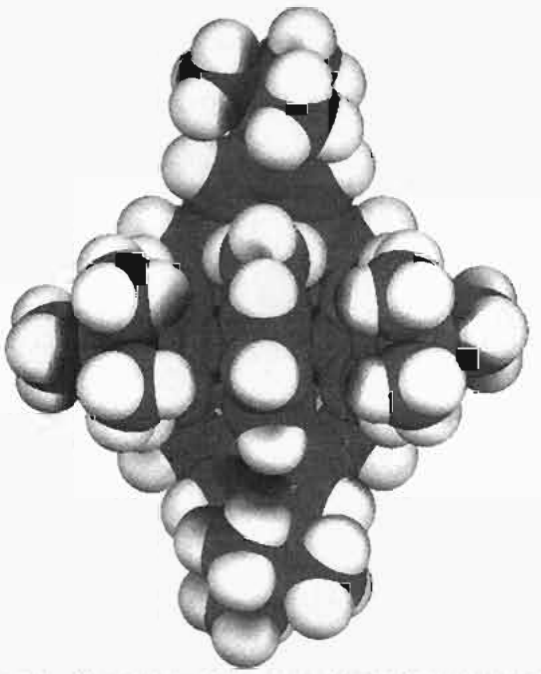

Figure 13. Space-filling diagram of [Cp*Ta(*p-tert*-butylcalix[4]-arene)]·toluene (**2a**·toluene), viewed into the calixarene pocket at the included toluene molecule.

associated with the $NCCH_3$ ligand suggest minimal perturbation from the bonding involved in free acetonitrile, which is not surprising since the d^0 Ta center in **2c** cannot π-back-bond into the antibonding π^* molecular orbitals of $NCCH_3$.[40] The N−C distances of N(10)−C(10) (1.110(7) Å) and N(20)−C(20) (1.124(7) Å) and N−C−C angles of 177.9(7)° for N(10)−C(10)−C(11) and 179.7(7)° for N(20)−C(20)−C(21) indicate an N−C bond order of 3. Although no other Ta(V) adducts of acetonitrile have been crystallographically characterized, similar features were observed in the solid state structures of other d^0 V(V) and Nb(V) complexes with acetonitrile, such as [V(=O)$(NO_3)_3CH_3CN$] (V−N = 2.24(3) Å)[41] and [Nb(=O)$(NCCH_3)_2Cl_3$] (Nb−N = 2.44(2) and 2.245(9) Å).[39]

(40) Collman, J. P.; Hegedus, L. S.; Norton, J. R.; Finke, R. G. *Principles and Applications of Organotransition Metal Chemistry*; University Science Books: Mill Valley, CA, 1987.
(41) Einstein, F. W. B.; Enwall, E.; Morris, D. M.; Sutton, D. *Inorg. Chem.* **1971**, *10*, 678.

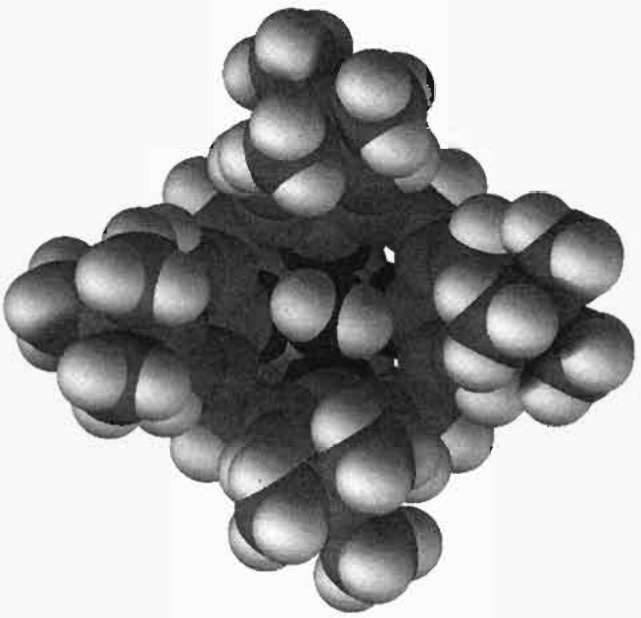

Figure 14. Space-filling diagram of [Cp*Ta(OH$_2$)(*p-tert*-butylcalix[4]arene)] (**2b**), viewed into the filled calixarene pocket.

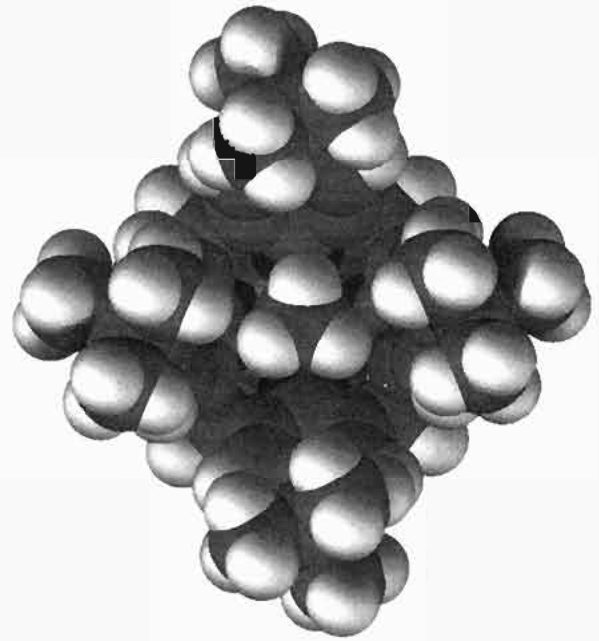

Figure 15. Space-filling drawing of [Cp*Ta(NCCH$_3$)(*p-tert*-butylcalix[4]arene)] (**2c**), viewed into the filled calixarene pocket.

The calixarene pocket of **2c** has approximately 4-fold symmetry, like that in **2b**. The *endo*-calix angles O(120)–Ta(100)–O(160) (155.8(2)°) and O(140)–Ta(100)–O(180) (155.3(2)°) are similar, as are the corresponding angles O(220)–Ta(200)–O(260) (155.2(2)°) and O(240)–Ta(200)–O(280) (155.7(2)°) of the second molecule in the asymmetric unit. The Ta–O_{calix} distances also fall in a narrow range (1.970(4)–2.007(4) Å). Similarly, the Ta–O_{calix}–C_{calix} angles vary only slightly, ranging from 130.1(3) to 136.1(3)°. There is also an approximately linear relationship between the Ta–O_{calix} distances and Ta–O–C_{calix} angles in complexes **2b** and **2c**, as depicted in the bottom of Figure 6, but with a narrower distribution of values compared to those of the more distorted complexes **1** and **2a** shown at the top of Figure 6.

As in the solid state structure of **2a**·2toluene·pentane, the presence of a Cp*Ta moiety on the rim of the calixarene pocket had a profound effect on the positioning of the included NCCH$_3$ molecule in **2c**. Here the electron-deficient metal center at the lower rim coordinates the lone pair of the N atom of acetonitrile, orienting it as indicated by **III**. This orientation is opposite to

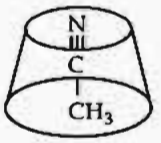

III

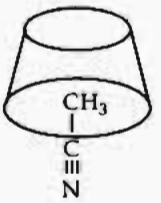

IV

that of a previously studied inclusion complex of acetonitrile by a calixarene macrocycle, [tetraethyl-*p-tert*-butylcalix[4]arene tetracarbonate]·NCCH$_3$, which is depicted as **IV**.[34] Positioned with the methyl group of the acetonitrile slightly deeper into the calixarene pocket, the closest *endo*-calix interaction of this organic clathrate is 3.80 Å and occurs between a bridgehead aromatic carbon and the acetonitrile methyl carbon. The closest bridgehead carbon-to-methyl carbon distance in either of the two molecules of **2c** is 4.06 Å.

Space-filling diagrams of the calixarene pockets of **1**, **2a**, **2b**, and **2c** are shown in Figures 12–15,[42] respectively, highlighting the elliptical shapes of **1** and **2a** compared with the circular nature of **2b** and **2c**. It is also clear that the toluene, water, and acetonitrile molecules are nestled tightly in the calixarene pockets in **2a–c**, at least in the solid state. A summary of all intracalixarene and -cyclopentadienyl distances is presented in Table 10. These values are in agreement with others in the literature.

Fenske–Hall Calculations and Packing Considerations. Fenske–Hall calculations were carried out to address two issues. We wished to determine the orbitals available for binding nucleophiles in the *endo*-calix position and also to identify changes in metal–ligand interactions that occurred with the switch from approximately 2-fold symmetry in **1** and **2a** to 4-fold symmetry in **2b** and **2c** in the solid state. Symmetry designations have been omitted because the Cp* and calixarene ligands combine to give only C_s symmetry.

Figure 16 shows the relevant valence orbitals of the [Cp*Ta]$^{4+}$ and [calix[4]arene]$^{4-}$ fragments as well as the resulting molecular orbitals in [Cp*Ta(calix[4]arene)], **1**. In order to focus on bonding within the metal–calixarene fragment, we neglect the Cp*–Ta interactions in this discussion. Detailed descriptions of such metal–cyclopentadienyl bonding interactions are available elsewhere, and results for the present molecules are generally consistent with these analyses.[40,43,44] The calixarene fragment oxygen σ_{p_z} orbitals overlap well with the metal $d_{x^2-y^2}$ orbital generating σ-bonding orbital 77 and σ^* antibonding orbital 127. Only the former is filled, resulting in a strong bonding interaction. The metal hybrid orbital 34, designated hy, is approximately half Ta s and half Ta p_z in character; this and the d_{z^2} orbital are virtually uninvolved in calixarene binding. π-Bonding between the phenoxide oxygen and tantalum atoms conceivably could use both the vertical, π_v, and horizontal, π_h,

(42) Space-filling diagrams were generated with the Chem-Ray graphics program (Lauher, J. W. *J. Mol. Graphics* **1990**, *8*, 34) supplied as a part of the teXsan program package: Single Crystal Structure Analysis Software, Version 1.6.

(43) Elian, M.; Chen, M. M. L.; Mingos, D. M. P.; Hoffmann, R. *Inorg. Chem.* **1976**, *15*, 1148.

(44) Lauher, J. W.; Elian, M.; Summerville, R. H.; Hoffmann, R. *J. Am. Chem. Soc.* **1976**, *98*, 3219.

Table 10. Average Intracalixarene Distances (Å) for **1** and **2a–c**[a]

	1	2a	2b	2c-1[b]	2c-2
Cp* C–CH_3					
range	1.480–1.496	1.491–1.511	1.494–1.500	1.491–1.508	1.489–1.506
mean	1.490(6)	1.499(8)	1.497(3)	1.500(7)	1.498(8)
Cp* C–C					
range	1.421–1.425	1.410–1.421	1.403–1.427	1.396–1.418	1.408–1.428
mean	1.423(2)	1.416(5)	1.414(9)	1.406(8)	1.419(9)
calix C–C					
range	1.371–1.415	1.377–1.406	1.376–1.410	1.371–1.411	1.382–1.411
mean	1.39(1)	1.392(7)	1.400(9)	1.39(1)	1.396(7)
calix H_2C–C					
range	1.502–1.524	1.499–1.528	1.505–1.534	1.510–1.524	1.510–1.527
mean	1.512(6)	1.514(9)	1.52(1)	1.517(5)	1.518(5)
calix C–O					
range	1.340–1.379	1.350–1.366	1.350–1.367	1.356–1.366	1.343–1.376
mean	1.36(2)	1.360(7)	1.358(8)	1.360(4)	1.36(1)
tBu H_3C–C					
range		1.448–1.535	1.511–1.541	1.48–1.54	1.52–1.544
mean		1.52(2)	1.532(8)	1.52(2)	1.530(8)
tBu $(H_3C)_3C$–C					
range		1.536–1.543	1.529–1.540	1.533–1.546	1.525–1.534
mean		1.54(3)	1.534(5)	1.542(7)	1.529(4)

[a] Distances reported have not been corrected for thermal motion. Standard deviations quoted for mean values are those for the given populations. [b] **2c** contains two molecules in the asymmetric unit, denoted here **2c-1** and **2c-2**.

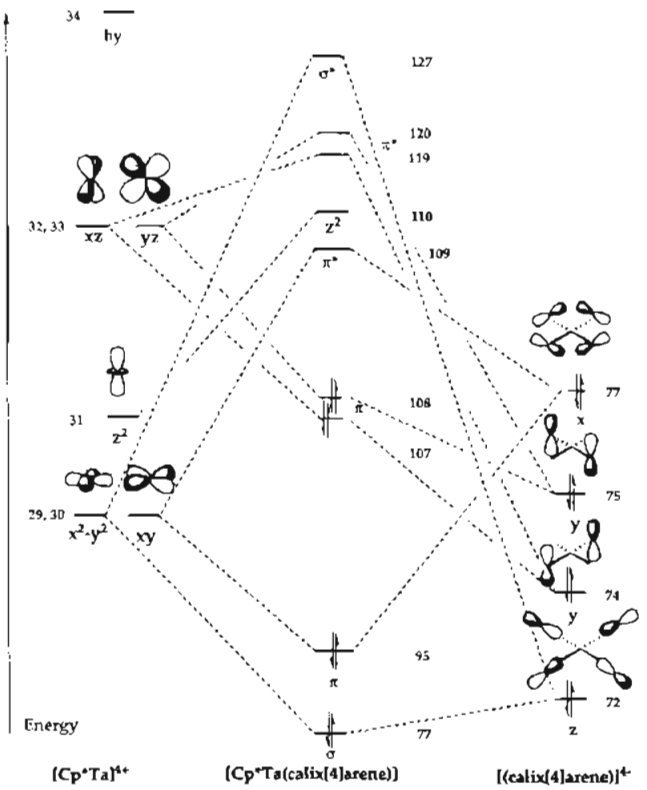

Figure 16. Overlap of $[Cp^*Ta]^{4+}$ with $[(calix[4]arene)]^{4-}$ fragment orbitals to form molecular orbitals of [Cp*Ta(calix[4]arene)], **1**. Only orbitals involved in metal–calixarene bonding are shown. Orbital numbers are shown next to each level. The label "hy" represents a hybrid of 55% Ta s and 40% Ta p_z. Energy separations are not drawn to scale. Precise values are listed in Table 11.

sets from the calixarene ligand, corresponding to the phenoxide oxygen p_y and p_x orbitals, respectively. There is some mixing of the calix π_v orbitals with the metal d_{xz} and d_{yz} orbitals, but these latter orbitals are primarily involved in Cp* bonding and mix only to a small extent with the calixarene. The π_h orbitals combine with the tantalum d_{xy} orbital to form much stronger π interactions with the phenoxide oxygens, however, generating the filled π orbital, 95, and the empty π^* orbital, 109. These interactions are shown in **V** and **VI**. The HOMO of the complex

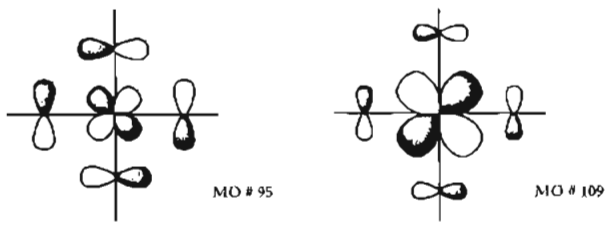

V VI

is primarily calix[4]arene ligand-based whereas the LUMO is primarily d_{xy} in character. The next highest unoccupied molecular orbital has mostly d_{z^2} character. The steric bulk of the pentamethylcyclopentadienyl ligand prohibits reactions in the *exo*-calix position involving either orbital. The steric requirements of the calix[4]arene ligand also prohibit σ donor nucleophile binding to the d_{xy} orbital. Of the two lowest unoccupied MO's, which are very close in energy, only the d_{z^2} orbital is geometrically available, and it is of appropriate symmetry to interact in the *endo*-calix position with filled p_z orbitals of nucleophiles.

The results of Fenske–Hall calculations on the representative complexes [Cp*Ta(OH_2)(calix[4]arene)] and [Cp*Ta($NCCH_3$)-(calix[4]arene)] are shown in Figure 17. The bonding interaction of a nucleophile with complexes such as [Cp*Ta(calix[4]arene)], **1**, shown on the left side of Figure 17, is predominantly through the d_{z^2} orbital. The interaction of the s/p_z hybrid hy is minimal and is not shown. Upon binding of either H_2O or H_3CCN, the d_{z^2} orbital is extensively mixed in a σ fashion with an O/N p_z orbital, whereas the π^* orbital is virtually unperturbed. The quantitative energy changes for these orbitals upon guest binding are summarized in Table 11.

As shown in Figures 3 and 4, in both **1** and **2a** the C(20)–C(25) and C(60)–C(65) arene rings are canted upward, forcing O(20) and O(60) closer to Ta than O(40) and O(80). The result is a reduction of local symmetry for the calixarene ligand from C_{4v} to C_{2v}. For comparison with the Fenske–Hall study of **1**, the model complex [Cp*Ta(calix[4]arene-C_{4v})] was also studied, in which the calix fragment has precise C_{4v} symmetry. The energies of the relevant frontier orbitals are listed in Table 11.

Table 11. Comparison of Molecular Orbital Energies for [Cp*Ta(calix[4]arene)] (**1**), [Cp*Ta(calix[4]arene-C_{4v})], [Cp*Ta(OH_2)(calix[4]arene)], and [Cp*Ta($NCCH_3$)(calix[4]arene)]

	[Cp*Ta(calix[4]arene)]		[Cp*Ta(calix[4]arene-C_{4v})]		[Cp*Ta(OH_2)(calix[4]arene)]		[Cp*Ta($NCCH_3$)(calix[4]arene)]	
orbital	MO no.	energy (eV)	MO no.	energy (eV)	MO no.	energy (eV)	MO no.	energy (eV)
σ^*	127	20.369	127	19.876	131	20.494	137	20.902
d_{z^2}	110	−1.069	110	−1.637	125	9.440	132	10.60
π_2^*	109	−1.426	109	−1.742	113	−1.346	116	−0.953
π_2	108	−10.895	108	−10.778	112	−10.645	115	−9.656
π_1	95	−15.382	95	−15.517	98	−15.246	102	−14.962
σ	77	−18.439	77	−18.829	80	−18.464	82	−18.550
p_z (B)					56	−22.19	68	−20.920
$\lvert\Delta E\rvert_{\pi-\pi^*}$		13.956		13.775		13.900		14.009
HOMO−LUMO gap (eV)		9.470		9.036		9.300		8.703

Table 12. Mulliken Atomic Charges from Fenske−Hall Calculations for [Cp*Ta(calix[4]arene)], **1**, [Cp*Ta(calix[4]arene-C_{4v})], [Cp*Ta(OH_2)(calix[4]arene)], and [Cp*Ta($NCCH_3$)(calix[4]arene)]

atom	[Cp*Ta(calix[4]arene)]	[Cp*Ta(calix[4]arene-C_{4v})]	[Cp*Ta(OH_2)(calix[4]arene)]	[Cp*Ta($NCCH_3$)(calix[4]arene)]
$\delta_{O(20)}$	−0.526	−0.555	−0.591	−0.587
$\delta_{O(40)}$	−0.602	−0.555	−0.618	−0.597
$\delta_{O(60)}$	−0.499	−0.553	−0.584	−0.599
$\delta_{O(80)}$	−0.594	−0.557	−0.588	−0.581
Ta	1.889	1.882	1.925	1.921
O/N			−0.342	−0.389

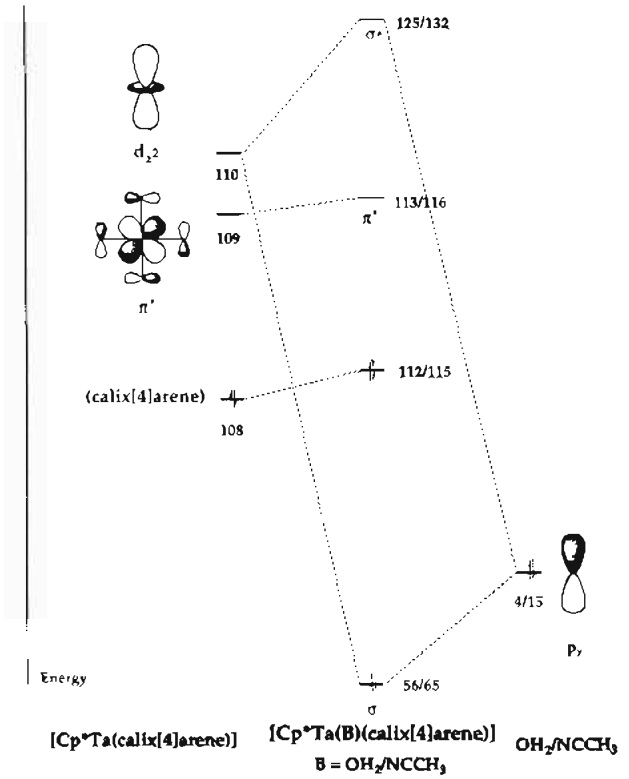

Figure 17. Orbital overlap of [Cp*Ta(calix[4]arene)], **1**, with nucleophiles H_2O and CH_3CN to give the complexes [Cp*Ta(OH_2)(calix[4]-arene)] and [Cp*Ta($NCCH_3$)(calix[4]arene)]. Orbital numbers are shown next to each level. Energy separations are not drawn to scale. Precise values are listed in Table 11.

Of particular interest is the decrease in HOMO−LUMO gap by 0.434 eV in [Cp*Ta(calix[4]arene-C_{4v})] from that of **1**, implying greater stability in the distorted calixarene.

The π-bonding interaction of MO 95 plays a significant role in the stabilization of the distorted calixarene. The energy gap between the π and π^* orbitals is 0.181 eV greater in **1** than in [Cp*Ta(calix[4]arene-C_{4v})]. Thus the 2-fold distortion seems to provide better overlap of the calix π_h orbitals with the d_{xy} orbital. The bonding π orbital is higher in **1** than in [Cp*Ta-(calix[4]arene-C_{4v})], but the antibonding orbital is even more destabilized, resulting in a net gain in stabilization for **1** compared with [Cp*Ta(calix[4]arene-C_{4v})]. Thus there is greater PhO → Ta π-donation in **1** from the π_h calixarene orbital into the Cp*Ta d_{xy} orbital.

The relative partial charge on each phenoxide oxygen atom is also a measure of the postulated PhO → Ta interactions, since less negative charge results from more electron donation to the metal center, and *vice versa*. A summary of these partial, or Mulliken, atomic charges is presented in Table 12. The partial charges for O(20) and O(60) are distinctly less negative than those on O(40) and O(80) for the "empty pocket" complex [Cp*Ta(calix[4]arene)] (**1**). In contrast, the partial charges on O(20)−O(80) for the complexes [Cp*Ta(OH_2)(calix[4]arene)] and [Cp*Ta($NCCH_3$)(calix[4]arene)], which contain ligands in the *endo*-calix site, are all essentially the same and more negative than the charges on O(20) and O(60) of **1**. Thus less electron density is donated to the metal center from the phenoxide atoms, and the *endo*-calix ligand provides additional electrons, resulting in only slightly greater net positive charge on the tantalum centers after nucleophile binding. These data support our intuition that O(20) and O(60) in the "empty pocket" and electron-deficient complexes **1** and **2a** donate more electron density than O(40) and O(80), distorting the calixarene macrocycle from 4-fold to 2-fold symmetry in the solid state.

Since all four phenoxide oxygen atoms are potential π donors, it is not obvious a priori why **1** and **2a** should distort in the manner observed, despite the fact that the Fenske−Hall calculation offers some insight into how the bonding adjusts to take advantage of the distortion. We suggest, on the basis of studies with CPK molecular models, that canting of all four rings simultaneously would not be possible owing to restrictions by the methylene tethers. Similarly, donation from two cis oxygen atoms would force crowding of two arene rings. Since these steric constraints of the calixarene methylene-tethered phenols influence the amount of distortion that can take place, shortening of two trans Ta−O bonds represents a compromise between the electronic requirements of the d^0 metal center and the limited flexibility of the macrocycle. Upon binding of a nucleophile, in the "filled pocket" complexes **2b** and **2c**, less PhO → Ta electron donation is required and, consequently, less distortion of the calixarene ligand occurs.

As discussed earlier, the packing diagram of **1** reveals insertion of two Cp* methyl groups from one molecule into

the pocket of a neighboring calixarene. These interactions occur parallel to the O(20)−Ta−O(60) vector, which has the shortened Ta−O bonds. The included toluene molecule in the structure of **2a** is similarly aligned along this same vector. Crystal-packing forces thus contribute to this 2-fold distortion. The resulting distortion of the calixarene satisfies the electronic requirements of the tantalum center in a manner that complements these solid-state packing interactions.

Conclusions

Transition metal calixarene complexes [Cp*Ta(calix[4]arene)] (**1**), [Cp*Ta(*p-tert*-butylcalix[4]arene)] (**2a**), and [CpNb(*p-tert*-butylcalix[4]arene)] (**3**) have been prepared and characterized. These mononuclear complexes have electron-deficient metal centers which are protected from reaction in the *exo*-calix position by the bulky cyclopentadienyl and pentamethylcyclopentadienyl ligands but have an available site for nucleophile binding in the *endo*-calix site. The structural characterization of [Cp*Ta(calix[4]arene)] (**1**) and [Cp*Ta(*p-tert*-butylcalix[4]-arene)] (**2a**) revealed an elliptical distortion of the 4-fold symmetry of the starting calixarene macrocycles in the solid state upon binding the electron-deficient tantalum center. Insight into how this distortion of the calixarene ligand in **1** and **2a** alters the metal−phenoxide π interactions was provided by Fenske−Hall calculations. This distortion facilitates the unusual sideways positioning of toluene in the *endo*-calix toluene position in [Cp*Ta(*p-tert*-butylcalix[4]arene)]·2 toluene·pentane (**2a**)·2 toluene·pentane. Intermolecular interactions occur in the solid state structure of **1**, in which the Cp* methyl groups penetrate the calixarene pocket of a neighboring complex. Nucleophile binding in the *endo*-calix site occurred in the solid state structures of [Cp*Ta(OH_2)(*p-tert*-butylcalix[4]arene)] (**2b**) and [Cp*Ta($NCCH_3$)(*p-tert*-butylcalix[4]arene)] (**2c**). These transition metal calixarene products combine the attractive forces of the ligand pocket with the electrophilicity of an electron-deficient metal center to promote binding within the calixarene basket.

Acknowledgment. This work was supported by a grant from the National Science Foundation. We thank Professors Tong Ren and Tomoaki Tanase for helpful discussions.

Supplementary Material Available: Tables of hydrogen positional parameters and *B*(eq) values, anisotropic thermal parameters, and complete interatomic bond distances and angles for [Cp*Ta(calix[4]-arene)] (**1**), [Cp*Ta(*p-tert*-butylcalix[4]arene)] (**2a**), [Cp*Ta(OH_2)(*p-tert*-butylcalix[4]arene)] (**2b**), and [Cp*Ta($NCCH_3$)(*p-tert*-butylcalix-[4]arene)] (**2c**) (49 pages). Ordering information is given on any current masthead page.

IC941356C